^{4}He experiments can serve as a data base for determining the three–nucleon force

H. M. Hofmann

Institut für Theoretische Physik III, University of Erlangen-Nürnberg,

Staudtstraße 7, D 91058 Erlangen, Germany

G. M. Hale

Theoretical Division, Los Alamos National Laboratory, Los Alamos, NM 87545, USA

Abstract

We report on microscopic calculations for the ^{4}He compound system in the framework of the resonating group model employing realistic nucleon-nucleon and three nucleon forces. The resulting scattering phase shifts are compared to those of a comprehensive R-matrix analysis of all data in this system, which are available in numerical form. The agreement between calculation and analysis is in most cases very good. Adding three-nucleon forces yields in many cases large effects. For a few cases the new agreement is striking. We relate some differences between calculation and analysis to specific data and discuss neccessary experiments to clarify the situation. From the results we conclude that the data of the ^{4}He system might be well suited to determine the structure of the three-nucleon force.

Introduction

For the nucleon-nucleon system the Nijmegen-group [1] has developed a database of some 5600 data points for the proton-proton and neutron-proton scattering. All modern nucleon-nucleon potentials have to be tested against this dataset and yield a χ^2 per degree-of-freedom of the order of one before they are generally accepted. For the three-nucleon force (TNF) the natural system are the three-nucleon systems ^{3}H and ^{3}He. In these two cases, however, realistic nucleon-nucleon (NN) forces allow to describe the deuteron-nucleon scattering data already quite well [2] and the TNF yield only minor corrections for an almost perfect reproduction of the data, except for the notorious A_y problem [3]. But even to cure the A_y problem only small changes of the deuteron-nucleon P-wave phase shifts of the order of a degree are sufficient to reproduce the low-energy data [4]. At higher energies, which we do not consider here, TNF effects are more pronounced; see [5]. Also, three-body breakup reactions might be a more sensitive test [6, 7, 8]. In this situation, another system can be helpful to determine the TNF, if such a system were accessible to scattering calculations employing realistic two- and three-nucleon forces. Furthermore, the available amount of data must be of the order of that of the NN system. At the moment computer power limits the scattering calculations in the many channel case to a mass number below 6. For the three systems, ^{4}H, ^{4}He, and ^{4}Li, scattering calculations using realistic NN forces exist [9, 10, 11, 12]. Partially also TNF have been employed. The second criterion is only met by the ^{4}He system. The two-body scattering channels triton-proton, ^{3}He-neutron, and deuteron-deuteron allow for elastic scattering and various reactions, with cross section measurements and also many polarization observables existing. Due to well developed resonances [13] their energy dependence is sometimes rather strong. About 5000 individual data are the input for the ongoing R-matrix analysis [14], a number large enough to allow for detailed comparison with calculations using various forces.

In this paper we report on microscopic calculations using realistic nuclear forces, comparing the results for scattering phase shifts with those of the R-matrix analysis on a partial-wave-by-partial-wave basis and then to a selected set of data. This set of data is chosen to demonstrate the agreement to be reached by the analysis and the parameter free calculation, but also to indicate the neccessity of new or better data in order to improve the R-matrix analysis and to allow for a more detailed comparison with the calculated results. The format

of the paper follows to a large extent that of earlier work [10] using a rather old version of the Bonn potential [15] expanded in terms of Gaussians [16]. We first discuss the essentials of the refined resonating group model (RRGM) used here. Then we describe briefly the R-matrix analysis, which is ongoing work from the evaluation [13], and discuss changes since the last publication. A detailed comparison of diagonal scattering phase shifts and reaction matrix elements from the analysis with the calculated ones comprises the next section. The following section discusses how well data can be reproduced by the R-matrix analysis and the calculation, and which conclusions about the underlying interaction are possible. Finally the quest for new or better data for selected experiments is discussed, especially which kind of information might be drawn from them. We conclude the paper by a discussion about the suitability of the dataset as a measure for determining the structure of the TNF.

I. RGM AND MODEL SPACE

We use the resonating group model [17, 18] in its refined version [19] to compute the scattering in the ^{4}He system using the Kohn-Hulthén variational principle [20]. The main technical problem is the evaluation of the many-body matrix elements in coordinate space. The restriction to a Gaussian basis for the radial dependencies of the wave function allows for a fast and efficient calculation of the individual matrix elements [18, 19]. However, to use these techniques the potentials must also be given in configuration space in terms of Gaussians. In this work we use suitably parametrized versions of the Argonne v18 (AV18) [21] NN potential, and the Urbana IX (UIX) [22], and V_3^* proposed in [23] and used in [24], NNN potentials.

In the ^{4}He system we use a model space with six two-fragment channels, namely the p - ^{3}H, the n - ^{3}He, the d - ^{2}H, the d - ^{2}H (S=0), the đ resonance, the đ - đ , and the (pp) - (nn) channels. The last three are an approximation to the three- and four-body breakup channels that cannot in practice be treated within the RRGM. The ^{4}He is treated as four clusters in the framework of the RRGM to allow for the required internal orbital angular momenta of ^{3}H, ^{3}He or ^{2}H.

For the scattering calculation we include all S-, P-, D-, and F-wave contributions to the $J^\pi = 0^+, 1^+, 2^+, 3^+, 4^+, 0^-, 1^-, 2^-, 3^-$, and 4^- channels. From the R-matrix analysis these channels are known to reproduce the low-energy experimental data. The full wave function

for these channels contains over 100 different spin and orbital angular momentum configurations, hence it is too complicated to be given in detail. The RRGM can be considered as a kind of variational calculation, hence, increasing the model space used usually improves the calculation. During the work we increased the model spaces several times. Due to the amount of material to be shown, we present here only results obtained for the largest model space. Some results obtained for smaller spaces are given in [25] and [26]. Using a genetic algorithm [27] for AV18 and UIX together, and allowing for S-, P-, and D-waves on all internal coordinates we found a triton binding energy of -8.460 MeV for dimension 70. This practically converged result compares favorably with the numerically exact one of Nogga [28] of -8.478 MeV. Since the Gaussian width parameters were optimized for NN and NNN interaction together, the agreement for the AV18 alone is only -7.57 MeV, compared to the exact one of -7.62 MeV [28]. Since isospin is a good approximation in light nuclei, we use for the ^{3}H and ^{3}He the same internal configurations and the same width parameters; however, the coefficients are (slightly) different due to the Coulomb force (and to a minor extent isospin-breaking terms in the AV18 potential). Note, that all calculations are done for physical channels, and not for channels with good isospin. For the deuteron we used 5 width parameters for the S-wave and 3 for the D-wave, yielding -2.213 MeV, just 10 keV short of the experimental value of -2.2245 MeV. The binding energies and relative thresholds for the various potentials are given in table I. For NN and NNN together the experimental binding energies and thresholds are very well reproduced. The RGM can only deal with two-body channels. To mock up the break-up channels, we allowed for configurations containing $\vec{d}$, (pp), and (nn). Since these are unbound, any unrestricted variational calculation will produce a wave function of infinite extent and zero energy. To have a finite extent, we use the deuteron S-wave width parameters, and let only the coefficients vary, to give the lowest possible (positive) energy. This procedure yields as binding energies +0.818 MeV, +1.203 MeV, and +0.805 MeV, respectively. In the previous calculation [10] these channels had some visible influence on the calculated phase shifts. In the present calculations they could be neglected, due to the much larger model spaces, except for the binding energy of the ^{4}He ground state, where they contribute 100 keV or 150 keV for AV18 alone and the TNF included.

This representation of ^{3}H/^{3}He , deuteron and the unbound NN systems form the model space of the ^{4}He scattering system. We get for the different J^π values up to 10 physical chan-

TABLE I: Comparison of experimental and calculated total binding energies and thresholds relative to $^3\mathrm{H} - p$ (in MeV) for the various potential models used

potential	E_{bin}			E_{thres}	
	^{3}H	^{3}He	^{2}H	$^3\mathrm{He} - n$	$d - d$
AV18	-7.572	-6.857	-2.213	0.715	3.145
AV18 + UIX	-8.460	-7.713	-2.213	0.747	4.033
AV18 + UIX $+V_3^*$	-8.452	-7.705	-2.213	0.747	4.025
exp.	-8.481	-7.718	-2.224	0.763	4.033

nels, insufficient to find reasonable scattering results. So-called distortion or pseudo-inelastic channels [18] without an asymptotic part have to be added to improve the description of the wave function within the interaction region. For this purpose all the configurations calculated for the physical channels except one per channel can in principle be reused, keeping only those width parameters which describe the internal region. In practice, however, this works only for a bound state calculation. In scattering calculations, the numerical accuracy in manipulating large matrices introduces some small amount of noise into the calculated results, e.g. phase shifts. Therefore we omit from each physical channel two to five components, to avoid the noise completely. This procedure reduces the binding energy of the ground state of ^{4}He by typically 20 keV, relative to the full bound state calculation. In the following we will always give the energies from the scattering calculation.

Recently Fonseca [29] pointed out that states having a negative parity J_3^- in the three-nucleon fragments increase the $n-^3$H cross section noteably. Contrary to the neutron-triton system we found in the ^{4}He system that the inclusion of such distortion states in the preliminary small model space calculations gave minor effects compared to adding UIX. Therefore in the converged calculation we did not allow for such states, in order to save computational resources, as we had anyhow to deal with sometimes more than a thousand channels.

II. R-MATRIX ANALYSIS

The Coulomb-corrected, charge-independent R-matrix analysis of the ^{4}He system from which the various "experimental" phase shifts are obtained in this paper is similar to the one described in Section 3 of our previous publication [10]. It uses the approximate charge independence of nuclear forces to relate the parameters in charge-conjugate channels, while allowing simple corrections for the internal Coulomb effects.

The isospin $T = 1$ parameters were taken from an analysis of p - ^{3}He scattering data [14] that gives a good description of all data at proton energies below 20 MeV. The $T = 1$ eigenenergies $E_\lambda^{T=1}$ are, however, shifted by the internal Coulomb energy difference $\Delta E_C = -0.64$ MeV, and the p - ^{3}H and n - ^{3}He reduced-width amplitudes $\gamma_{c\lambda}^{T=1}$ are reduced by the isospin Clebsch-Gordan coefficient $1/\sqrt{2}$. The isospin $T = 0$ parameters are then varied to fit the experimental data for reactions among the two-fragment channels p - ^{3}H, n - ^{3}He, and d - ^{2}H, at energies corresponding to excitations in ^{4}He below 29 MeV. In this fit, the $T = 0$ nucleon-trinucleon reduced-width amplitudes are constrained by the isospin relation $\gamma_{n\,^3\mathrm{He}}^{T=0} = -\gamma_{p\,^3\mathrm{H}}^{T=0}$, and a small amount of internal Coulomb isospin mixing is introduced by allowing $\gamma_{dd}^{T=1} \neq 0$, which is neccessary to reproduce the differences between the two branches of the d - d reaction. The charge-independent constraints imposed on the parameters of this model might be too simple, and although the R-matrix results given here are not yet final, they represent the most comprehensive and detailed attempt to date to give a unified phenomenological description of the reactions in the ^{4}He system. Note, that the R- and S-matrices are always represented in physical channels, and the isospin arguments are only used to reduce the number of parameters in the R-matrix.

A summary of the channel configuration and data included for each reaction is given in table II. New data have been added in most of the reactions, including the neutron total cross sections of refs. [30, 31, 32, 33], the elastic scattering cross sections of [34], and the ^{3}H(p, n) reaction cross-section measurements of [35, 36].

When the S-matrix is continued onto the complex energy surface, near one of its poles it has the form

$$S = i\frac{\rho_0 \rho_0^T}{E_0 - E} \tag{1}$$

where $E_0 = E_R - i\Gamma/2$ is the complex pole energy and ρ_0 is the complex residue amplitude. A procedure for obtaining E_0 and ρ_0 from R-matrix parameters is given in [37]. The expec-

TABLE II: Channel configuration (top) and data summary (bottom) for each reaction in the ^{4}He system R-matrix analysis

Channel	$l_{\max}$	a_c (fm)
^{3}H - p	3	4.9
^{3}He - n	3	4.9
^{2}H - d	3	7.0

Reaction	Energy range (MeV)	# Observable types	# Data points
$^3\mathrm{H}(p,p)^3\mathrm{H}$	$E_p = 0 - 11$	3	1382
$^3\mathrm{H}(p,n)^3\mathrm{He}$ + inv.	$E_p = 0 - 11$	5	856
$^3\mathrm{He}(n,n)^3\mathrm{He}$	$E_n = 0 - 10$	2	397
$^2\mathrm{H}(d,p)^3\mathrm{H}$	$E_d = 0 - 10$	6	1666
$^2\mathrm{H}(d,n)^3\mathrm{He}$	$E_d = 0 - 10$	6	921
$^2\mathrm{H}(d,d)^2\mathrm{H}$	$E_d = 0 - 10$	6	399
	totals:	28	5621

tation of the Breit-Wigner approximation is that the sum of the partial widths is related to the imaginary part of the pole energy by

$$\rho_0^\dagger \rho_0 = \Gamma. \tag{2}$$

For the resonances in light systems such as ^{4}He, this is often not the case [37, 38]. As explained in [37], a parameter characterizing the strength of an S-matrix pole,

$$\mathcal{S} = \frac{\rho_0^\dagger \rho_0}{\Gamma}, \tag{3}$$

in terms of the magnitude of its residue compared to its displacement from the real axis, can be quite different from unity for poles that do not show up as strong resonances in the data.

III. PHASE SHIFT COMPARISONS

Since the nuclear many-body forces are not yet well enough established, we cannot anticipate that a direct comparison between calculation and data leads to clear conclusions,

especially as the complicated, time consuming calculations do not allow for easy modifications of the potentials used.

It is enough that the matrix elements of one partial wave are not reproduced well enough, to spoil any agreement between calculation and data. In this situation the comprehensive R-matrix analysis, which takes into account all physical channels simultaneously, connects elastic scattering data with reactions and interpolates in energy, is an absolute must. This interpolation is neccessary to study energy dependencies and the effect of, even broad, resonances.

We can write each S-matrix element connecting channels a and b as $\langle a, l_a, S_a | S^{J^\pi} | b, l_b, S_b \rangle = \eta e^{2i\delta}$, where η and δ depend on the channels a and b, their orbital angular momenta l_a and l_b, their channel spins S_a and S_b, and the total angular momentum J and parity π.

In the following we will compare in most cases only diagonal scattering phase shifts δ and only sometimes present results for the coupling strength η, in order not to be swamped with too many data. In addition all S-matrix elements to a given J^π-value have to obey unitarity; hence, diagonal and non-diagonal matrix elements are always related.

For most energies we have to deal with a coupled channels problem. Only below the ^{3}He - n threshold at 700 keV the triton-proton 0^+, 0^-, 3^+, and 4^- channels are single channels indeed. In this energy range, due to the low energy, the P-wave channels are still dominated by the threshold behavior, showing only small phase shifts. The D- and F-waves are even smaller, below 0.1 degrees. The 0^+ channel, however, is dominated by the first exited state in ^{4}He. The R-matrix analysis yields a rapidly increasing phase shift, which crosses the 90-degree line 100 keV below the threshold, reaching about 105 degrees at threshold in a cusp-like manner, to slowly decrease afterwards, as shown in fig. 1. The corresponding pole of the S-matrix is found much below, close to the triton-proton threshold at a complex energy of 0.114 - i0.196 MeV.

The calculations started with the AV18 NN potential alone. With increasing model space, the ^{4}He binding energy converged at -24.090 MeV. All calculations showed qualitative agreement with the R-matrix results; the smallest model space is above the R-matrix results, an increased one well below - see fig.1 in ref.[25] - and the converged model space yields quantitative agreement, as shown in fig.1. The corresponding S-matrix has in the low-energy region two complex energy poles, given in table III. The lower one is close to the one

TABLE III: Pole positions of the 0^+ S-matrix from the multi-level R-matrix analysis compared to the results of the various potential models used. All energies are given in MeV

R-matrix		AV18			AV18 + UIX			AV18 + UIX +V_3^*		
E_R	$\Gamma/2$	E_R	$\Gamma/2$	$\mathcal{S}$	E_R	$\Gamma/2$	$\mathcal{S}$	E_R	$\Gamma/2$	$\mathcal{S}$
0.114	0.196	0.198	0.256	1.40	0.105	0.129	1.54	0.091	0.077	1.52
		0.497	2.114	0.06	0.664	2.227	0.17	0.574	2.229	0.14

found in the R-matrix analysis.

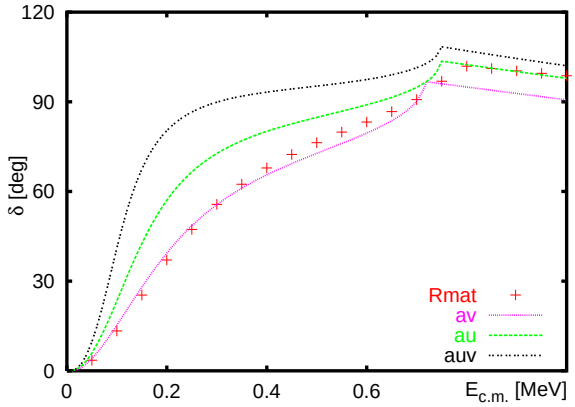

FIG. 1: (Color online) Low-energy triton-proton 0^+ phase shifts calculated using AV18 (av), AV18 and UIX (au), and additionally V_3^* (auv) compared to R-matrix (Rmat) results.

For a well isolated resonance the modulus of the residue of the S-matrix at the pole position $E_R - i\Gamma/2$ in the single channel case is just Γ, dictated by unitarity. As most of the resonances in ^{4}He are broad and overlapping, this criterion is not met in most cases, see the previous section and [13] for a more detailed discussion. In order to indicate the relevance of a complex energy pole of the S-matrix, we present in table III the pole positions found, together with the ratio $\mathcal{S}$ of the modulus of the residue and Γ for an easier comparison.

The real part of the calculated poles closest to the threshold is by no means related to that energy, where the corresponding phase shift crosses 90 degrees; see fig.1. The second pole found in all the calculations has a small ratio $\mathcal{S}$, which means it cannot be a standard Breit-Wigner resonance as discussed in [13]. These findings indicate the overlapping of (many) resonances. Furthermore, reducing the model space slightly changes the positions of

all poles strongly, except for the lowest one. Usually we find many more poles (with small strength) in the S-matrix calculation than in the R-matrix analysis, whose influence on the physical observables is expected to be weak. The next pole in the R-matrix analysis is above 3 MeV. In this interval more poles of the S-matrix are found.

Since neglecting the Coulomb force shifts the lowest pole below the ^{3}H - p threshold, so that it becomes a particle-stable state (see also [39] for various NN forces and [12] for additional NNN forces), we discuss the situation in more detail. For AV18 alone this state is bound relative to the threshold by 62 keV, for AV18 and UIX by 112 keV. Therefore in these cases, the 0^+ ^{3}H - p phase shift has to fall with energy and cannot reproduce the R-matrix results.

In order to sketch the intriguing situation we display the two 0^+ S-matrix poles closest to the ^{3}H - p threshold in fig.2 for the AV18 alone and the full interaction.

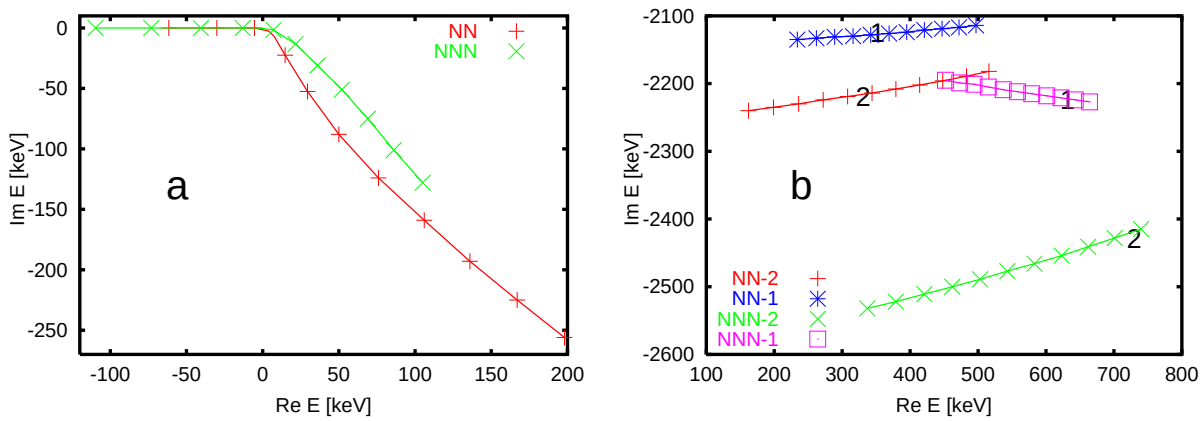

FIG. 2: (Color online) Complex energy pole positions of the 0^+ S-matrix for a) the first pole and b) the second pole. The ticks indicate the strength of the Coulomb potential on a 0.1 grid, starting with zero most strongly bound; for details, see text.

For the AV18 alone the second 0^+ state starts just below -60 keV on the real axis, becomes unbound slightly above a strength of the Coulomb potential of $C = 0.2$, then moves gradually into the complex energy plane up to a real part of the energy of about 200 keV. This pole is characterized by a residue that is always larger than required by the unitarity condition on the real axis by up to a factor of 1.9, close to the ^{3}H - p threshold, falling to 1.4 for the full Coulomb interaction.

Employing now also the Urbana IX potential the situation is quite similar, as shown in

fig. 2a. Since the second 0^+ state is more strongly bound without the Coulomb force, it becomes only unbound for a strength in excess of $C = 0.35$, then starting to move into the complex plane at a somewhat slower pace, but with a similar pattern as for AV18. The residue is up to a factor of three larger than required by unitarity. Note, that all the resonant states are well below the corresponding ^{3}He - n threshold. They are all on the unphysical Riemann-sheet adjacent to the physical Riemann-sheet, with one channel only open.

In table III we find the next pole in energy still below the ^{3}He - n threshold for the full Coulomb strength. These states, however, are not analytically connected to those found for no Coulomb interaction. Except for a small splitting of 60 keV, due to the isospin breaking terms in the AV18 potential the ^{3}He - n and ^{3}H - p thresholds coincide for vanishing Coulomb interaction. Hence, the unphysical Riemann-sheet adjacent to the physical sheet has two open channels. The corresponding pole positions are labeled with a "2" in fig. 2b. With increasing Coulomb strength, the real part of the pole position has to increase, due to the ^{3}He - n threshold moving to higher energies and thus reducing the attraction. We mark with "2" on the corresponding lines in fig. 2b, from which strength onward the adjacent Riemann-sheet has only one open channel. This means that the influence of these poles onto the observables on the real axis will be reduced. Accordingly, we label pole position on the one-open-channel Riemann-sheet with "1" and mark with "1" on the lines in fig. 2b, from which strength on this Riemann-sheet is adjacent to the physical one. For the AV18 alone this transition occurs around a strength of $C = 0.45$, yielding two poles with real energy positions close to the corresponding ^{3}He - n threshold, but far in the complex plane with small residues. Adding the UIX potential, the one-channel pole appears on the adjacent Riemann-sheet just above $C = 0.80$, whereas the two-channel pole disappears only for a strength $C = 0.97$. All the poles have very small residues, when they are on the adjacent sheet to the physical one.

So altogether we are faced in both calculations with the situation of two poles, one of which becomes a bound state increasing its residue when leaving the real axis, and the other has a much smaller residue than expected from a standard Breit-Wigner resonance. This is the only case that we encountered two S-matrix poles of the same angular momentum and parity so close together in energy. The behavior of the residues, one growing, one reduced when going into the complex plane makes it very difficult to predict their respective effects on the real axis, where they could be compared to experiment. We mention in passing,

that the exact position of the poles reacts very sensitive on the numerical procedures of inverting the big matrices or how the regularized Coulomb functions are expanded in terms of Gaussians.

Let us now discuss the behavior of the phase shifts, displayed in fig. 1, in more detail. We find the results for the AV18 NN interaction alone in almost perfect agreement with the R-matrix analysis below the ^{3}He - n threshold, despite the corresponding binding energy of ^{4}He missing 4 MeV. When the ^{3}He - n channel opens, a bit too early (see table I), the calculated triton-proton phase shift decreases slowly with energy.

Adding the UIX TNF force allows to reproduce the ^{3}He - n threshold much better, but below threshold the calculated phase shifts overshoot the R-matrix results quite a bit. Above the agreement is nice. The calculated binding energy of -28.294 MeV is almost at the experimental value of -28.296 MeV. With the additional TNF V_3^* the phase shifts are much too positive, the threshold is nicely reproduced and the ground state is overbound by 700 keV. This interaction, tailored to resolve the A_y problem in nucleon-deuteron scattering, hence, acting in relative P-waves only, is therefore not acceptable, and we will give no further results for this interaction. Furthermore, except for the above phase shifts and close to the ^{3}He - n threshold, the effects of this force are of minor importance. Directly above the ^{3}He - n threshold all potentials yield a linear fall off with energy.

Let us now discuss the higher energies. In [10] the phase shifts resulting from a version of the Bonn potential were discussed. The comparison of the diagonal phases from the calculation and the R-matrix analysis in fig. 5 of ref. [10] was not too convincing. Only an Argand plot revealed that the diagonal S-matrix elements become small due to a very strong coupling between the triton-proton and the ^{3}He - n channel to form a state of good isospin T = 0. Therefore the influence of these matrix elements on physical observables is weak.

In fig. 3 we display the calculation for the AV18 potential alone in comparison with the results from the R-matrix analysis used in 1997 [10] and a recent one from 2003 [14]. The differences in the data input into these two analysis are discussed above. The obvious change in the data between the analysis from 1997 and 2003 is in the triton-proton and ^{3}He - n phases. Above 5 MeV they come close to each other as already predicted in the old calculation [10] and differ no more by 180 degrees as before. The $^1S_0$ d - d phases became more repulsive close to the threshold. The other change is the sign flip in the $^5D_0$ d - d

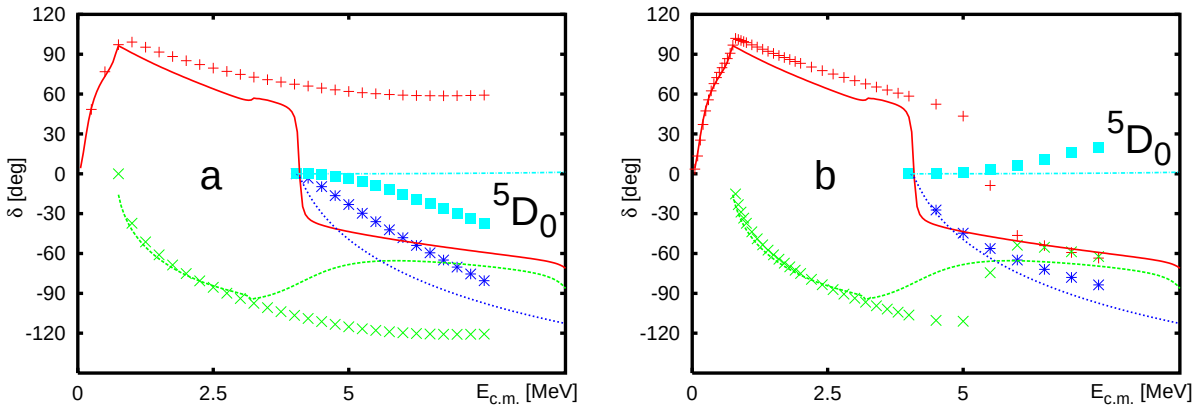

FIG. 3: (Color online) Elastic 0^+ phase shifts for all physical two-fragment channels calculated for the AV18 potential alone. The RRGM $^1S_0$ phase shifts are displayed as full lines (red) for the t - p ones, as dashed lines for the ^{3}He - n ones (green), and as dotted lines for the d - d ones (blue). The corresponding R-matrix results are given by $+$ for t - p, by x for ^{3}He - n, and by $*$ for d - d. We stick to this coding in this subsection where ever possible. The $^5D_0$ d - d phase shifts are especially marked. The RRGM calculated d - d phase shifts are shifted by 0.9 MeV to the experimental threshold. (a) The data from the R-matrix analysis are from 1997 as in [10]. (b) The data are from the R-matrix analysis from 2003.

channel. But these phases are small anyhow. The RRGM calculated results follow much more closely both R-matrix results up to about 3 MeV, compared to [10]. At the calculated d - d threshold there occurs a change in form. (Note that the calculated d - d phase shifts have been shifted in energy to the experimental threshold for an easier comparison. The tiny kink in the triton-proton phase shifts occurs at the calculated d - d threshold.) The energetic position of the calculated results are obviously wrong, due to the calculated d - d threshold being much too low; see table I. The qualitative behavior is encouraging. Since the only qualitative change in the R-matrix results of both analyses is in the 0^+ phase shifts and the quantitative changes in all other partial waves are too small to be clearly identified in the figures, we present in the following only results from the 2003 R-matrix analysis.

In fig. 4 we compare all physical 0^+ elastic scattering phase shifts calculated for AV18 together with UIX TNF with the recent R-matrix analysis. The agreement between this zero-parameter calculation and the analysis is remarkably good. As discussed above, the calculated low energy triton-proton phases are a bit too high, but from the ^{3}He - n threshold

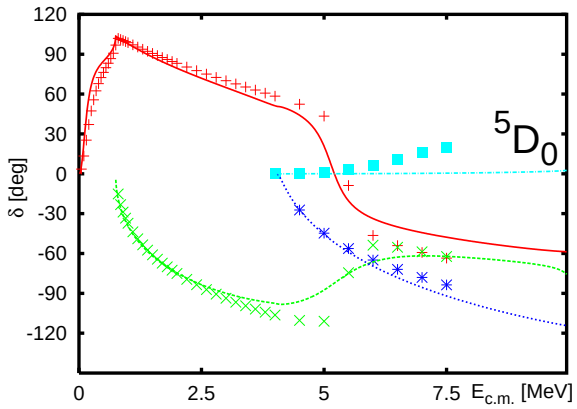

FIG. 4: (Color online) Elastic 0^+ phase shifts for all physical two-fragment channels calculated for the AV18 potential together with the UIX TNF. The coding of the lines and symbols is the same as in fig. 3.

up to the d - d threshold RRGM calculation and R-matrix analysis agree perfectly, then comes the rapid change in energy in the ^{3}H - p and ^{3}He - n phases, settling at similar values around 7 MeV. The $^1S_0$ d - d phase shifts are very well reproduced over the analyzed interval. Obviously these results do not leave too much room for modifications of the underlying NN and NNN potentials acting in the relative S-waves. The small values of the $^5D_0$ phases are not reached by the calculation.

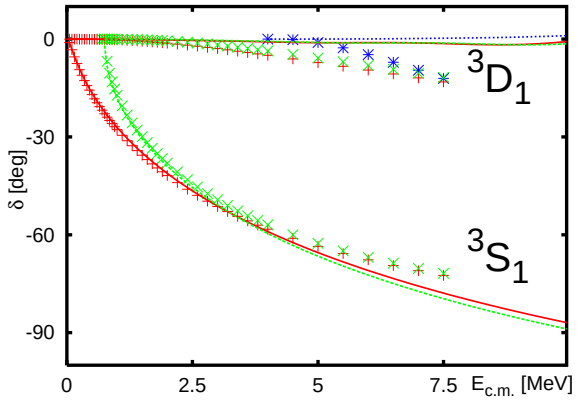

FIG. 5: (Color online) Same as fig. 3 but for the elastic 1^+ phase shifts calculated for the AV18 potential together with the UIX TNF.

Next we discuss the $J^\pi = 1^+$ partial waves. There the R-matrix analysis finds only one high lying resonance; see ref. [13]. In fig. 5 we compare the full calculation with the

analysis. All phase shifts from the R-matrix are negative. The D-wave ones are close to zero and do not reach -15 degrees, and the d - d ones are a bit more negative than in the earlier analysis; see fig.7 of ref. [10]. Both RRGM S-wave phase shifts agree nicely with the R-matrix results up to 6 MeV, above which the RRGM ones are a bit more repulsive than those from the analysis. The calculated D-wave phases are practically zero, the d - d ones slightly positive, the others negative, but do not reach the R-matrix values, which are small anyhow. Omitting these small phase shifts yields changes in the polarizations of typically 0.01, which is of the order of the experimental error bars for e. g. triton-proton scattering, but of the full data for deuteron-deuteron scattering, see section IV.

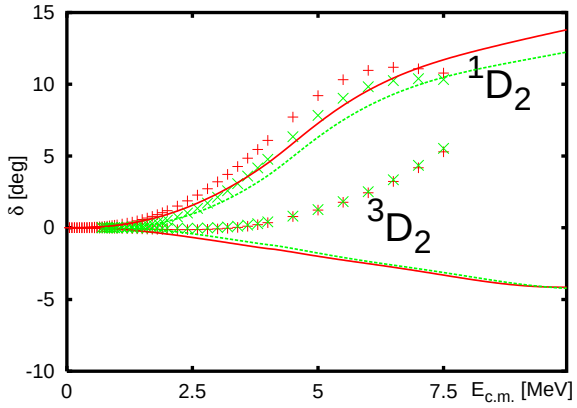

FIG. 6: (Color online) Comparison of the 2^+ t - p and ^{3}He - n phase shifts calculated for the AV18 potential together with the UIX TNF.

The 2^+ partial wave contains the most coupled channels. In the R-matrix analysis all possible D-waves and the $^5S_2$ d - d channel were taken into account. In the RRGM calculation the same physical channels and additionally, more than a thousand distortion channels are considered. Since all the D-wave phase shifts are small already, the $^5G_2$ d - d channel is neglected. In fig. 6 we compare the R-matrix [3 + 1] phase shifts with the calculated ones. All R-matrix phases appear to be positive, the $^1D_2$ just passing 10° with the t - p ones always a bit larger than the ^{3}He - n ones. The $^3D_2$ phases start out with tiny negative values up to -0.1 degree, before turning positive around 3 MeV, and barely reach 5°. All phases are slightly more positive than in the previous analysis [10]. The RRGM calculated $^1D_2$ phase shifts agree nicely with the analysis, a bit below at low energies, passing the R-matrix results at the end of the analyzed interval, but keep growing with energy, whereas

the R-matrix ones show signs of decreasing. The $^3D_2$ calculated phases are also small and yield very similar values for t - p and ^{3}He - n, but they disagree in sign with the R-matrix ones at higher energies. Since an earlier R-matrix analysis gave also a negative sign for these phase shifts, we were quite concerned, and tried to identify which of the additional data in the analysis might have introduced this sign flip. We could not find any polarization observable sensitive to the sign flip, and will come back to this point when discussing the comparison with data later on.

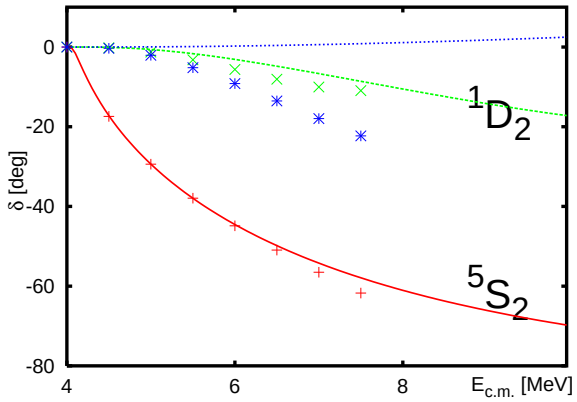

FIG. 7: (Color online) Comparison of the 2^+ d - d phase shifts calculated for the AV18 potential together with the UIX TNF. The $^5S_2$ are shown as full line (red) and +, the $^1D_2$ as dashed line (green) and x, and the $^5D_2$ as dotted line (blue) and $*$.

In fig. 7 we display the corresponding d - d phase shifts. The $^5S_2$ phases agree almost perfectly, fall off rapidly with energy, but not as much as in ref. [10]. The D-wave phase shifts are small. The values of both channels from the R-matrix turned negative; those from the RRGM calculation are essentially unchanged. The $^1D_2$ phase shifts agree very well between calculation and analysis; the $^5D_2$ do not, indicating a rather large J-splitting in the R-matrix analysis, and essentially none in the RRGM calculation.

For the 3^+ and 4^+ partial waves the R-matrix analysis finds small negative values for all D-wave phase shifts up to -5° for all physical channels. The RRGM results are even smaller. These small phase shifts have in most cases negligible effects on the observables, and are therefore not shown in a separate figure. Collecting, however, all ^3D_J triton-proton or ^{3}He-neutron or all ^5D_J deuteron-deuteron phase shifts from figs. 4, 5, 6, and 7 together with the results just mentioned, we find considerable J-splitting from the R-matrix analysis

and essentially none in the RRGM calculation. This is shown in fig. 8, where we display the triton-proton triplet D-wave phase shifts – the ^{3}He - n ones are similar – and the deuteron-deuteron quintet D-wave phase shifts. Note that at the same energy above the thresholds, the R-matrix analysis yields d - d phase shifts that are much larger, and show a much larger splitting than the triton - proton ones. it is remarkable that all the d - d phase shifts are negative, except for J = 0.

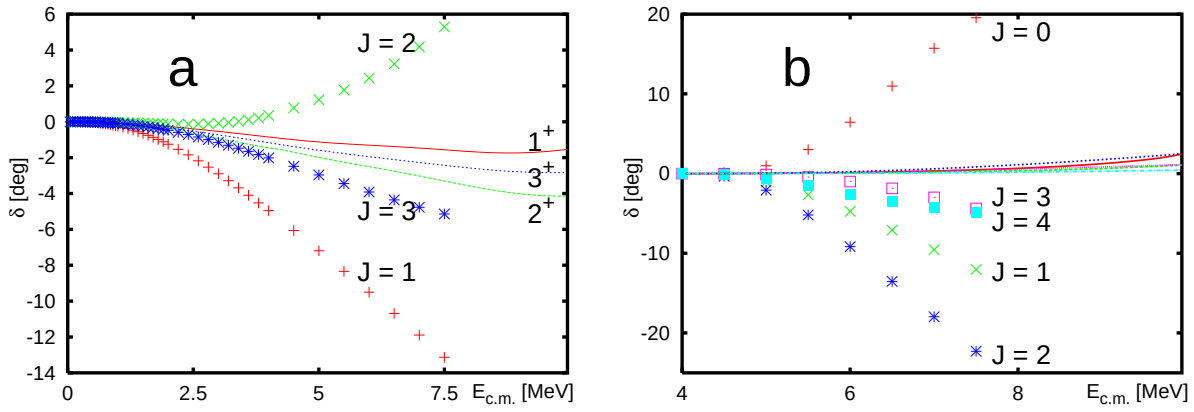

FIG. 8: (Color online) Comparison of the D-wave phase shifts for all possible total angular momentum values J for (a) triton-proton channels and (b) the deuteron-deuteron channels. Due to the smallness of the RRGM d - d phase shifts, we do not label them.

Let us summarize the results for the positive parities: Employing the AV18 and UIX potentials allows to reproduce all S-wave phase shifts for all fragmentations almost perfectly. Except for the 0^+ partial wave these are dominated by Pauli repulsion and, hence, negative. The singlet D-wave phase shifts agree nicely between analysis and calculation. For the ^3D_J [3 + 1] phase shifts, the R-matrix yields large J-splitting, with $^3D_1$ and $^3D_3$ negative, the other one positive. In a triton-proton optical model, such a splitting could be caused by a rather strong tensor force, but the actual values cannot be explained in a perturbative treatment.

The corresponding ^5D_J d - d phase shifts cannot be accounted for by deuteron-deuteron spin-orbit and tensor optical potentials, mainly due to the J = 0^+ phase shift being large and positive, and the J = 3^+ and J = 4^+ ones being small and negative. The RRGM calculation yields small negative values for the [3 + 1] phase shifts (see fig.8), and a splitting of the order of one degree, and for the d - d phase shifts, even smaller values, but

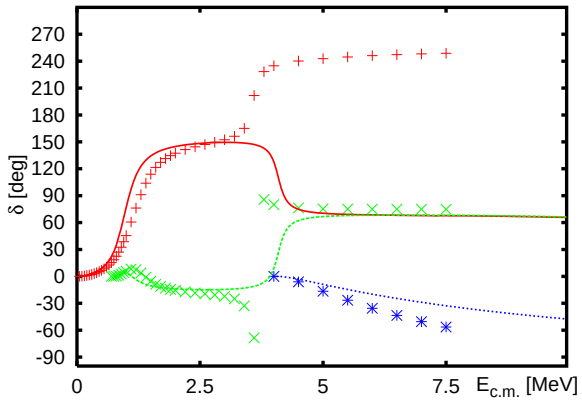

FIG. 9: (Color online) Same as fig. 3 but for the 0^- phase shifts. Above 4 MeV we added 180 degrees to the R-matrix ^{3}He - n phase shifts for an easier comparison with the RRGM results.

positive, with a similar splitting at comparable energies. These differences in the values of the phase shifts and their splittings are the main qualitative difference between R-matrix analysis and microscopic calculation for diagonal S-matrix elements. We will discuss this situation together with selected data at the end of the paper.

Let us now consider the negative-parity partial waves. The compilation [13] shows three 0^- resonances. Two of them can be easily read off from the rapid change with energy of the t - p and ^{3}He - n phase shifts in fig. 9. The third one of d - d structure is not obvious. Except for the regions where the [3 + 1] phases vary rapidly, the t - p and ^{3}He - n phase shifts differ essentially by irrelevant multiples of 180°. In the region of the first resonance, R-matrix and RRGM results agree nicely, but the position of the resonance seems to be a bit lower in the calculation. In the region of the second resonance, which seems to be somewhat higher in the calculation, the behavior of the R-matrix and RRGM phase shifts is completely opposite. Due to good isospin T = 1, this resonance leads to a strong coupling of the two [3 + 1] channels, with the coupling matrix element close to the unitary limit of one, leaving only a small value for the diagonal S-matrix element. The situation we find here is very close to that discussed previously [10] and is explained by the Argand plots displayed in figs. 11 and 12 of ref. [10], by showing the two S-matrices pass on different sides of the origin. Compared to the previous analysis and the calculation using the Bonn potential, the [3 + 1] phase shifts are now much better reproduced, the d - d ones are a bit underestimated; compare fig. 9 with fig. 10 of [10]. Since no more recent Bonn potential

is given in r-space, it could not be tested, if these differences are due to deficiencies of the older potential or to the much increased model spaces.

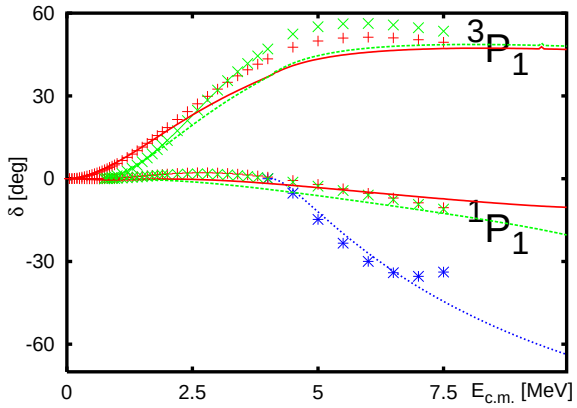

FIG. 10: (Color online) Same as fig. 5 but for the 1^- phase shifts.

The 1^- phase shifts are displayed in fig. 10. The extracted level structure is quite rich [13]. The [3 + 1] triplet phase shifts are positive, all others negative. The RRGM results agree favorably with the new R-matrix analysis. The difference in the [3 + 1] triplet phase shifts is much smaller than for the Bonn potential, as can be seen in fig. 13 of ref. [10]. The ^{3}He - n triplet phase shifts cross over the triton-proton ones at a higher energy and stay closer together in the calculation. The $^1P_1$ phases show a small splitting that is not found in the R-matrix analysis. Close to threshold, the d - d phase shifts are very well reproduced. The difference at the higher energies in the d - d phase shifts could be due to end-of-data effects in the analysis.

Since the $^3P_2$ phase shifts were the main culprit in [10] for missing most of the experimental values, we compare in fig. 11 the new calculation for the NN interaction alone and together with the TNF with the new analysis. The R-matrix values hardly changed; only the d - d phases became a bit less repulsive. Compared to the Bonn potential used in ref. [10], the RRGM results for the AV18 already are much more attractive, gaining 15 to 20 degrees at the higher energies. Also the moduli of the S-matrix elements are much closer to the R-matrix results than before. Adding the UIX TNF yields a small amount of further attraction. The R-matrix analysis allows also for F-waves. These can be coupled to $2^-, 3^-$, and 4^- partial waves. The resulting phase shifts turned out to be of the order of a few degrees in the energy range considered. Therefore, and due to a lack of computing

power, these partial waves were not calculated in [10]. During the comparison with data it turned out that all the ^{2}H(d,nucleon) analyzing powers depend sensitively on these small contributions and a description of the experimental situation is only possible if these partial waves are taken into account. Therefore every effort was made to calculate these. In fig. 11b we display the results of the calculations allowing also for the UIX TNF and the F-waves. The combined effect of coupling to F-waves and adding UIX TNF is additional attraction of the order of a few degrees.

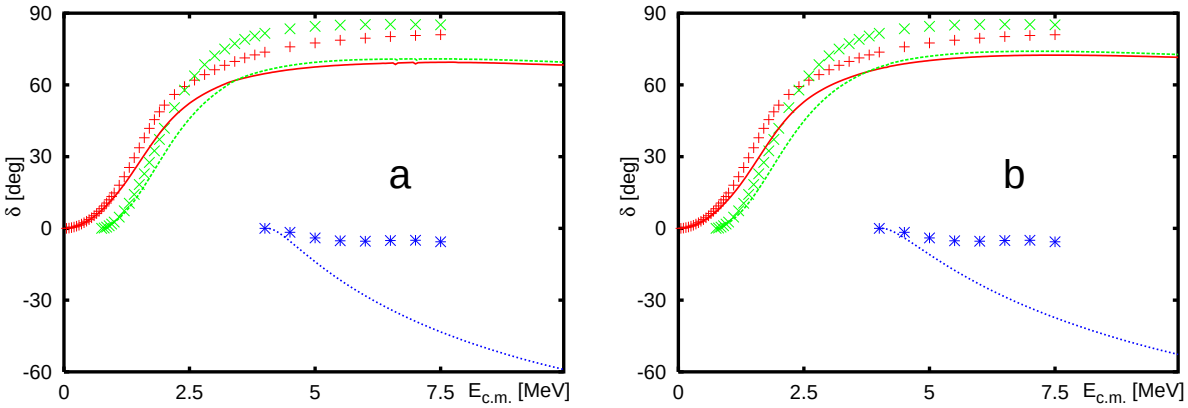

FIG. 11: (Color online) Comparison of the 2^- P-wave phase shifts. (a) Calculation for the AV18 alone, no coupling to F-wave allowed. (b) Calculation for AV18 and UIX including coupling to F-waves.

As for the 1^- channels, the ^{3}He - n phase shifts cross over the ^{3}H - p ones at a higher energy, and have less splitting in the calculation than in the R-matrix analysis. The d - d phase shifts from the analysis are close to zero, whereas the calculation yields similar values as for the 1^- channel. Altogether, the calculated [3 + 1] phase shifts are close to R-matrix ones, whereas the calculated d - d phase shifts do not reach the J-splitting found in the analysis. To make the situation more transparent, we compare in fig. 12 the calculated deuteron-deuteron P-wave phase shifts with those from the analysis.

As seen in fig. 12, the $^3P_1$ phase shifts agree nicely between calculation and analysis, and also the amount of splitting between the $^3P_1$ and $^3P_0$ phases is similar, but opposite in direction. The order of the different J-values is permuted. The $^3P_2$ phases vary widely between calculation and analysis, but due to the small phase shifts in the analysis we do not expect large effects omitting them altogether. Considering the three J-values together,

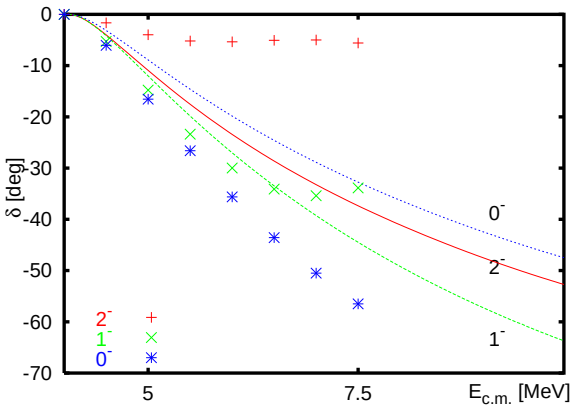

FIG. 12: (Color online) Comparison of the $d-d$ P-wave phase shifts. The calculations are for AV18 and the UIX potentials. The $^3P_2$ results are shown as full line (red) and +, the $^3P_1$ as dashed line (green) and x, and the $^3P_0$ as dotted line (blue) and $*$.

we find a reasonably large splitting in the analysis, hence, also reasonably large polarization data. From the small J-splitting of the calculated phase shifts, we expect small polarization data in d-d scattering. If the analysis and the direct calculation are to reproduce the same d-d data, the larger splitting in the R-matrix analysis has to be compensated by the results from higher partial waves, due to interference. We will come back to this point when discussing elastic deuteron-deuteron observables later in the paper.

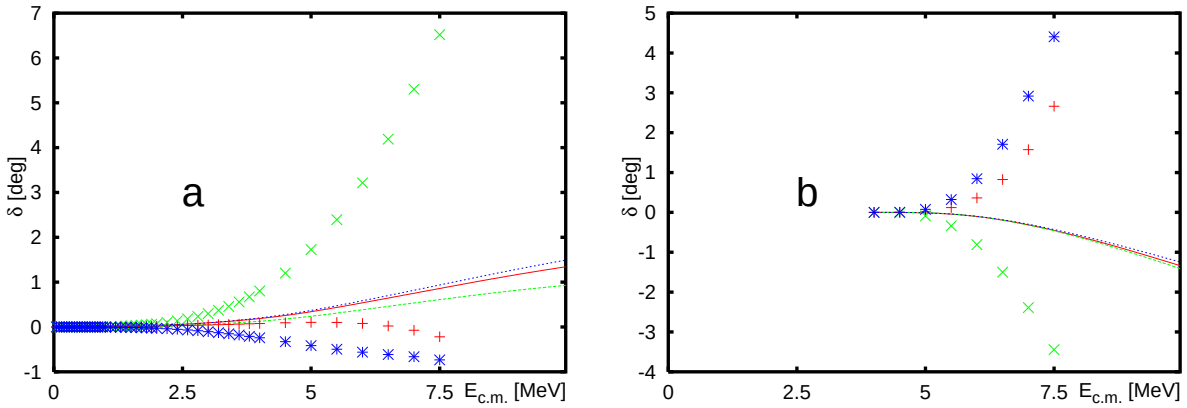

FIG. 13: (Color online) Comparison of the triplet F-wave phase shifts (a) for the triton-proton channels and (b) the deuteron-deuteron channels. The calculations are for AV18 and the UIX potentials. The $^3F_2$ results are shown as full line (red) and +, the $^3F_3$ as dashed line (green) and x, and the $^3F_4$ as dotted line (blue) and $*$.

In fig. 13 we display the F-wave phase shifts for the ^{3}H - p and d - d channels. Since the results for the ^{3}He - n channels are almost identical, we do not show them. The triton-proton R-matrix results are small, the $^3F_3$ phase shift being reasonably large and positive up to 7°, whereas the others are negative by less then 1 degree. The opposite sign of the $^3F_3$ phases could be due to a strong tensor force; however, the size of the $^3F_2$ and $^3F_4$ phases does not support this conjecture. The RRGM calculation yields essentially no J-splitting with all phase shifts slightly positive, up to one degree. We note in passing that the singlet F-wave phase shifts have the opposite sign to the $^3F_3$ ones, and about half the strength in the analysis and the calculation.

For the deuteron-deuteron channels the R-matrix analysis yields a reasonably large J-splitting with again the $^3F_3$ phase shift having the opposite sign of the rest. The RRGM calculation yields again essentially no splitting; all the phases are small and negative. This qualitative difference between R-matrix analysis and RRGM calculation seems much less important than for the D-waves because the values are much smaller; see, however, the discussion of the deuteron-deuteron analyzing powers below.

IV. DIRECT COMPARISON WITH EXPERIMENTS

In order to allow the Reader a direct comparison with the previous results obtained for the Bonn potential [10], we present figures for all the elastic scatterings and reactions presented there. We always use the results of the recent R-matrix analysis [14] and compare to the most complete calculations, i.e. using the AV18 NN potential alone and together with the UIX TNF potential and taking into account all S-, P-, D-, and F-wave matrix elements.

So contrary to [10], the R-matrix analysis and the RRGM calculation now consider exactly the same channels. When the inclusion of F-waves yields substantially different results, we also present those without F-waves. The RRGM calculation is done in 50 keV steps in the center-of-mass, starting from the ^{3}H - p threshold. This yields small deviations in energy from the experimental numbers, but the errors introduced by this procedure should be well within the size of the points used. The R-matrix analysis uses relativistic kinematics, the experimental threshold energies, and the correct energies of the data for the fit. Here we present results calculated for a varying energy grid, which uses values quite close to the experimental numbers, but calculated with non-relativistic kinematics. These small

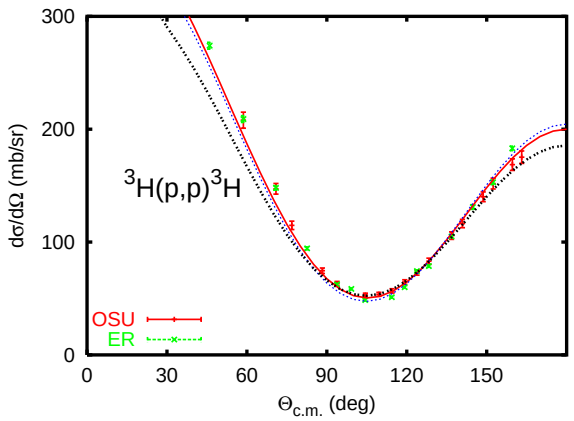

FIG. 14: (Color online) Differential elastic proton-triton cross section calculated at 3.1 MeV E_{cm}. The R-matrix results are shown as full line (red), the results from AV18 alone as thin dotted line (blue), and those for AV18 together with UIX as thick dotted line (black). We stick to this coding in the following where possible. The data are from Ohio State University (OSU) group [40] and from the Erlangen group [41]at 3.11 MeV.

differences do not play any significant role for the examples given in the following. We display first the data together with analysis and calculation as shown in [10], sometimes adding new data at the same energy. Then we discuss a few data sets that we consider critical to a further new analysis or to conclusions about the effects of TNF forces.

We present the various reactions in the order of the corresponding thresholds, starting with triton-proton elastic scattering. Around 4 MeV proton energy, differential cross section and analyzing-power measurements exist. In fig. 14 we compare the cross section data with the R-matrix analysis and the direct calculation. We see the data covering an angle range from about 45° to 160° in the center-of-mass system, with the Erlangen data [41] having the smaller errors, but disagreeing with the OSU data [40] at backward angles. The RRGM calculation is at an energy of 3.1 MeV in the center of mass, to be in agreement with the energy of the proton analyzing power; the R-matrix is at 3.0 MeV. These energy differences are too small to show any effect in the figures. The R-matrix reproduces the data quite nicely in general, and falls in between the data at the backward angles. For the AV18 potential alone, the RRGM yields results much better than for the Bonn potential [10], now almost agreeing with the R-matrix results, being slightly below at forward angles and slightly above at backward angles. Adding the UIX TNF destroys the good agreement.

Now the calculation is well below R-matrix and data at forward angles and also on the lower side for backward angles, but slightly above the data and analysis in the minimum region.

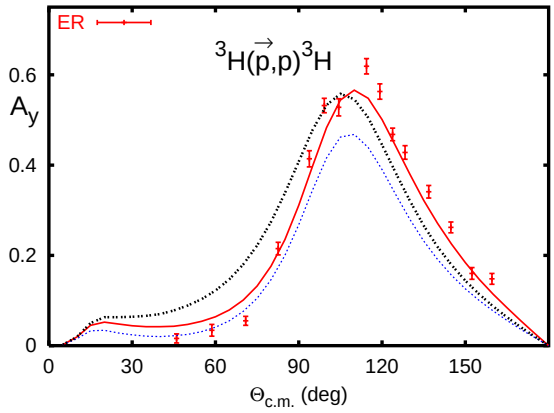

FIG. 15: (Color online) Proton analyzing power of the elastic scattering ^{3}H$(p,p)^3$H calculated at 3.1 MeV E$_{cm}$. The meaning of the lines is as in fig. 14. The data are from [41].

The proton analyzing-power data of the Erlangen group [41] cover the same angular range as the differential cross section; see fig. 15. The R-matrix analysis reproduces the data nicely, being slightly above the data for forward angles, just missing the maximum value, and barely reaching the data in the backward hemisphere. For the NN interaction alone, the RRGM calculation is always below the R-matrix analysis, closer to the data up to 70°, falls well below the maximum, and also well below all backward data. This situation appears similar to the notorious A_y problem in the A = 3 systems [3] and also to missing the maximum polarization value in p - ^{3}He scattering [24]. The full calculation, however, misses the forward data, but reaches the maximal value of the R-matrix analysis at a somewhat smaller angle, and thus falls below the backward polarization data. Note that we do not modify any S-matrix element, contrary to the previous calculations [10].

For elastic proton-triton scattering, triton analyzing-power data also exist from the Los Alamos group [42] at a close-by energy in the same angular range as the other data. The R-matrix just misses the negative values at forward angles; up to 80° it is somewhat above the data, but then agrees nicely with them, as shown in fig. 16. Using the AV18 alone yields triton analyzing powers just on top of the R-matrix results till its maximum, which is reached at a smaller angle and smaller value than R-matrix and data. Afterwards all calculated values are well below the data. Adding the UIX TNF yields much too high

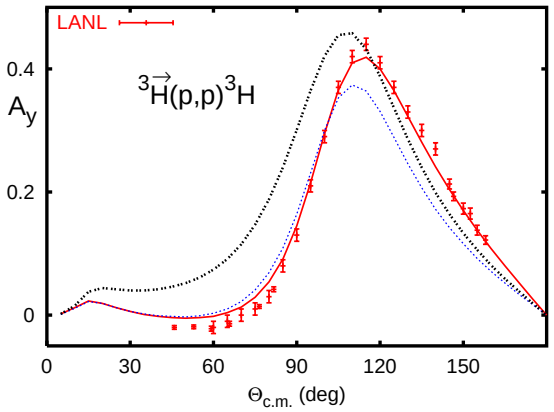

FIG. 16: (Color online) Triton analyzing power of the elastic scattering $^3\mathrm{H}(p,p)^3\mathrm{H}$ calculated at 3.2 MeV E_{cm}. The data at 3.21 MeV are from the Los Alamos group [42].

polarization values at forward angles, reaches the maximal data at a bit smaller angle, and falls below the data and R-matrix fit at backward angles. The large difference in the maximal proton and triton polarizations is caused by the rather large $^3P_1$ to $^1P_1$ transition matrix element.

Summarizing the results for elastic proton-triton scattering, we see large effects by adding UIX TNF, sometimes favorable, as for the maximal polarization values, and sometimes adverse, as for the differential cross section and the forward analyzing powers. Allowing in the calculation for F-waves and the 3^+ D-wave always improved the agreement between R-matrix and RRGM results, but in general the modifications were too small to display them clearly in figures. Contrary to the previous calculation [10], we cannot identify a single matrix element that causes the differences between the R-matrix analysis and the RRGM calculation. Usually the moduli agree within a few percent and the phase shifts within a few degrees. The only exception is the $^3P_0$ matrix element, which is small due to the strong coupling as discussed above. Adding the TNF increases it by a factor three to 0.22 and reduces its phase by 10°. Furthermore, the results for this partial wave vary strongly close to the energy considered; see fig. 9. The general structure of the differential cross-section and the two analyzing powers is already given by the three triplet P phase shifts and the $^3S_1$ ones. All the many others yield changes in the cross-section that are smaller than the difference between the R-matrix results and those of the full calculation. The differences in the analyzing powers at forward angles and around the maximum comes mainly from

the slightly differing $^3P_2$ matrix element and, to a lesser extent, from the size of the $^3P_0$ S-matrix element (the other two are so close that no differences are visible). Since the the maximal polarization values are reached by the full calculation also at higher energies, we do not see indications here of an "A_y problem", but we note that the forward analyzing powers are missed.

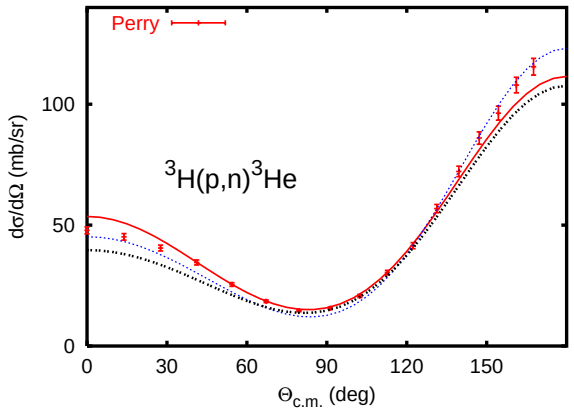

FIG. 17: (Color online) Differential cross section for the reaction ^{3}H$(p,n)^3$He calculated at 3.0 MeV E$_{cm}$. The data at 3.08 MeV are from Perry et al.[43].

The differential cross section for the reaction ^{3}H$(p,n)^3$He is shown in Fig. 17. The R-matrix analysis is somewhat above the very forward data and a bit below them at backward angles. The calculation for the AV18 potential alone reproduces the data very nicely, being only slightly below at forward angles. Adding the TNF destroys again the agreement, by loosing strength at forward and backward angles. All the large matrix elements agree between analysis and the calculations, with only the exception of the $^3P_1$ matrix element, which is above 0.2 in the R-matrix and in the full calculation, but only 0.04 for the AV18 alone. The modulus of this matrix element rises rapidly with energy from threshold to about 2.5 MeV E_{cm} above the triton-proton threshold in analysis and the full calculation, falling to a minimum near 5 MeV, and a gentle increase afterwards. The AV18 calculation, however, yields the maximum at 2 MeV, the minimum very close to zero just above 3 MeV, and a rather rapid increase afterwards. These rapid variations of this matrix element are the main reason for the rather strong energy dependence of the observables of the ^{3}H$(p,n)^3$He reaction. In addition, the moduli of the D-wave matrix elements increase rapidly with energy, thus leading to major changes within 200 keV, especially in polarization observables

TABLE IV: Comparison of experimental and calculated real and imaginary scattering lengths (in fm) for the potential models used

potential	a_0		a_1	
	$\Re$	$\Im$	$\Re$	$\Im$
AV18	7.776(1)	-5.019(1)	3.447(1)	-0.0066(1)
AV18 + UIX	7.622(1)	-4.095(1)	3.311(1)	-0.0051(1)
R-matrix	7.400(3)	-4.449(1)	3.286(6)	-0.0012(2)
exp.	7.370(58) [45]	-4.448(5) [46]	3.278(53) [45]	-0.001(2) [46]
exp.	7.456(20) [44]		3.363(13) [44]	

not displayed here. The final results are thus determined by many small matrix elements that change rapidly with energy, rather than by the large 0^- and 0^+ ones at the unitary limit. Unfortunately, all the polarization data are concentrated below 3.5 MeV, and none exist around 7.5 MeV, where all D-waves belong to the large matrix elements in the analysis.

The time-reversed reaction ^{3}He(n,p)^{3}H is used at low energies as a neutron standard reaction. These integrated cross sections are reasonably well reproduced by the current calculation (see [26], where an early version of the present calculations is reported). The main emphasis of [26], however, was the determination of the spin-dependent scattering lengths a_s of ^{3}He-neutron elastic scattering. In the meantime a new measurement of the coherent neutron scattering length exists [44] in addition to the recent measurement of the incoherent one [45]. Due to numerical problems we could hardly go down to 1 keV in the early RRGM calculations in order to determine the complex scattering lengths. Special measures had to be taken to extract them from the calculated S-matrix elements. Increasing the numerical stability by the procedure described in the beginning, we can now go down safely to 0.1 keV and check the extrapolation at even lower energies. The real part of a_s can now be calculated via the standard expression $a = \tan\delta/k$, whereas the imaginary part of a_0 still needs the expression given in [26]. The calculated results for a_1 are within the errors given in [26]. Since the measured coherent and incoherent scattering lengths are linear combinations of a_0 and a_1, and therefore always need the input of other data, we compare in tab. IV the calculated values with the extracted data.

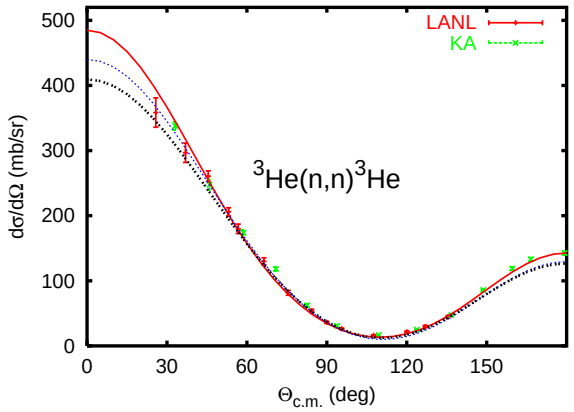

FIG. 18: (Color online) Differential cross section for the elastic scattering ^{3}He(n,n)^{3}He calculated at 6.0 MeV E_{cm}. The data are from Drosg [47] at 5.93 MeV and from the Karlsuhe-group [48] at 6.0 MeV.

We note in passing that the calculated coherent scattering length for the full calculation agrees perfectly with the new measurement [44]. Since the calculation, however, yields the spin-zero and spin-one parts separately, this agreement has to be considered fortuitious. The most recent measurement puts the spin-dependent scattering lengths well outside the older error bars.

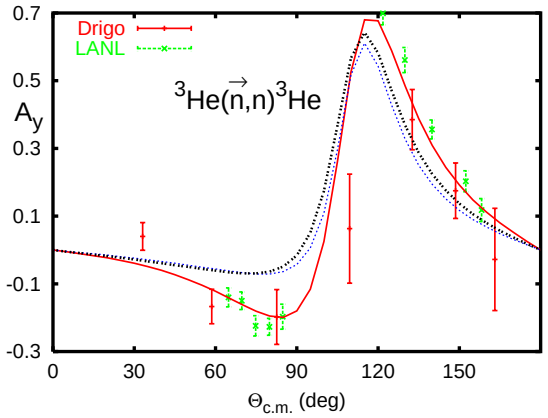

FIG. 19: (Color online) Neutron analyzing power for the elastic scattering ^{3}He(n,n)^{3}He calculated at 6.0 MeV E_{cm}. The data are from Drigo [49] and LANL [50] at 5.85 MeV and 6.0 MeV respectively.

For elastic ^{3}He-neutron scattering, cross section and analyzing-power data do not exist at the energy used for triton-proton scattering. In figs. 18 and 19 respectively, we display

such data, measured close to 6 MeV E_{cm}. The R-matrix analysis reproduces the cross section and analyzing-power data very well. The RRGM calculations do not reach up to the Karlsruhe cross sections [48] with their tiny errors at backward angles. Also the negative analyzing powers below 90° are not reached, the maximum is slightly missed, and they fall below the data at backward angles. Despite the similarity of the results with and without TNF, individual matrix elements turn out to be quite different in phase and/or modulus, but some changes reduce the polarization, others increase it, resulting in an almost zero net change. The differences between R-matrix analysis and the calculations are mainly due to the larger triplet-P phase shifts, shown in figs. 11, 10, and 9, which increase the cross section at forward and backward angles and yield strongly negative analyzing powers near 90°. Due to the higher energy, the $^3P_0$ matrix element has increased by a factor of 2 compared to triton-proton scattering, and therefore lost some of its sensitivity. The positive $^3D_2$ phase shift from the R-matrix, fig. 6, compensates for this large P-wave by reducing the maximal analyzing power and the 180° cross section. As in the triton-proton scattering, the three triplet P phase shifts and the $^3S_1$ one determine the overall structure of cross section and analyzing power, but here, due to the higher energy, the effects of the other matrix elements are larger for the cross section. For the analyzing powers the effectsof these other matrix elements are visible only in the fall-off from the maximum. The maximal polarization values are almost reached by the calculations.

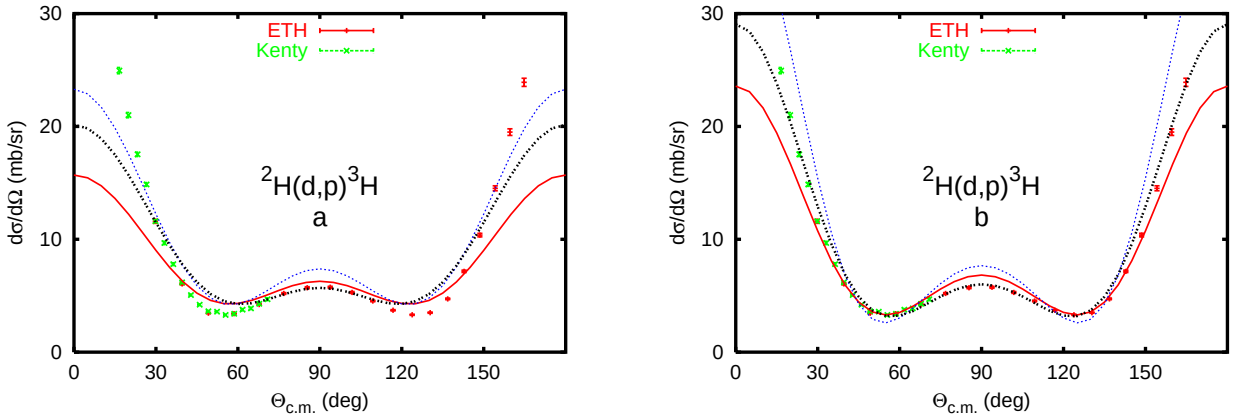

FIG. 20: (Color online) Differential cross section for the reaction $^2\mathrm{H}(d,p)^3\mathrm{H}$ calculated at 2.0 MeV E_{cm}. The data are from the Zürich group [51] and from the Kentucky group [52] at 2.0 MeV. For AV18 alone the energy is chosen in such a way that it agrees in the exit channel with the experimental one. F-waves are not taken into account in a, but in b.

Let us now discuss the deuteron induced reactions. In fig. 20 the ^{2}H$(d,p)^3$H differential cross section is displayed without and with F-waves taken into account. Without F-waves only the pure NN-only calculation comes close to the data, whereas with F-waves the data are rather nicely reproduced. The R-matrix analysis underestimates the cross section at the extreme forward and backward angles and overestimates it around 90 degrees. For the AV18 potential alone, the cross section is mostly overpredicted, but including the TNF yields results on top of the data. Due to the identical particles in the entrance channel the cross section has to be symmetric about 90°, which is not quite true for the two different data sets at the extreme angles. The forward Kentucky data are about 10 percent above the corresponding Zürich data at backward angles, which is revealed by comparing to the full calculation. We postpone the discussion of the effects of individual transition matrix elements until we have compared also all analyzing powers for this reaction, in order to avoid unneccessary repetition.

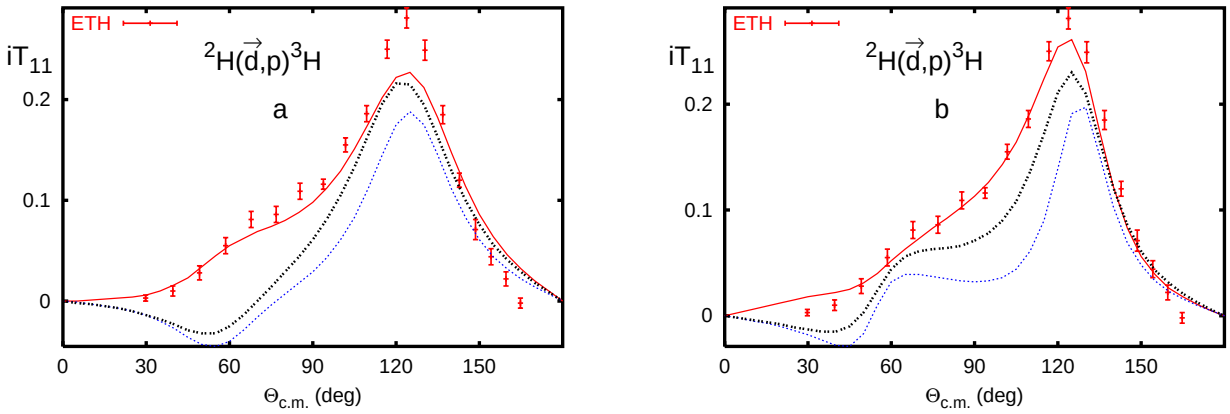

FIG. 21: (Color online) Same as fig. 20 but for the analyzing power iT_{11} of the reaction ^{2}H$(d,p)^3$H calculated at 2.0 MeV E$_{cm}$. The data at 2.0 MeV are from the Zürich group [51], as all the following polarization data.

The vector analyzing power is displayed in fig. 21. The R-matrix analysis does a nice job of reproducing most of the data. Without F-waves, the forward hemisphere data are well reproduced, the maximum is not reached, and the very small values above 150° are missed. Including F-waves, the data are very well reproduced, except for the zero values at forward and backward angles, and maybe also in the maximum. The RRGM calculations yield negative polarizations for forward angles, contrary to data; adding TNF makes the

results always more positive, as do the additional F-waves in the forward hemisphere. So the full calculation comes closest to the data, but cannot be called a good description of them. The AV18 calculation without F-waves yields only qualitative agreement.

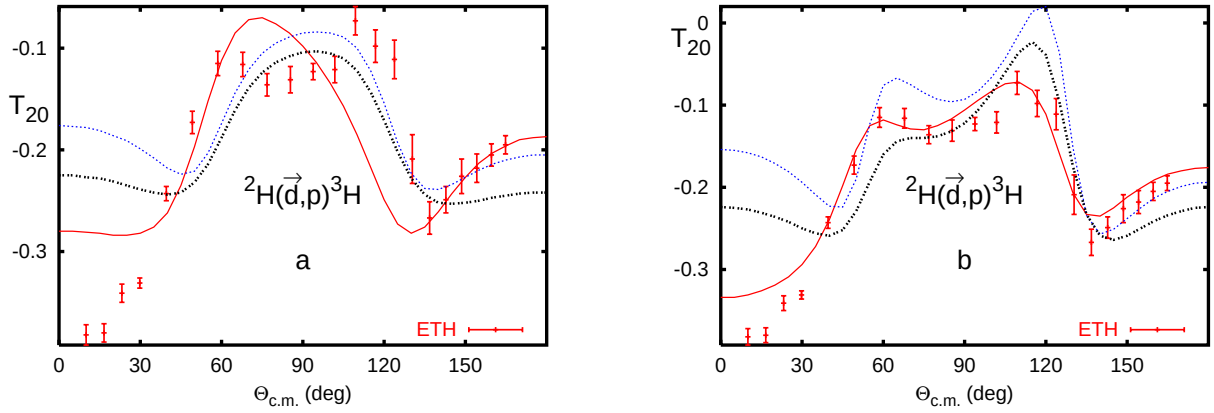

FIG. 22: (Color online) Same as fig. 21, but for the analyzing power T_{20} of the reaction ^{2}H$(d,p)^3$H

The T_{20} analyzing power is displayed in fig. 22. Without F-waves the double hump structure of the data is completely missed, and also the very negative values below 30 degrees. Including F-waves, the R-matrix analysis reproduces the data very well except for the forward angles. Both RRGM calculations miss the forward data totally. The AV18 alone overestimates the double hump structure, and including TNF improves the reproduction of the data somewhat.

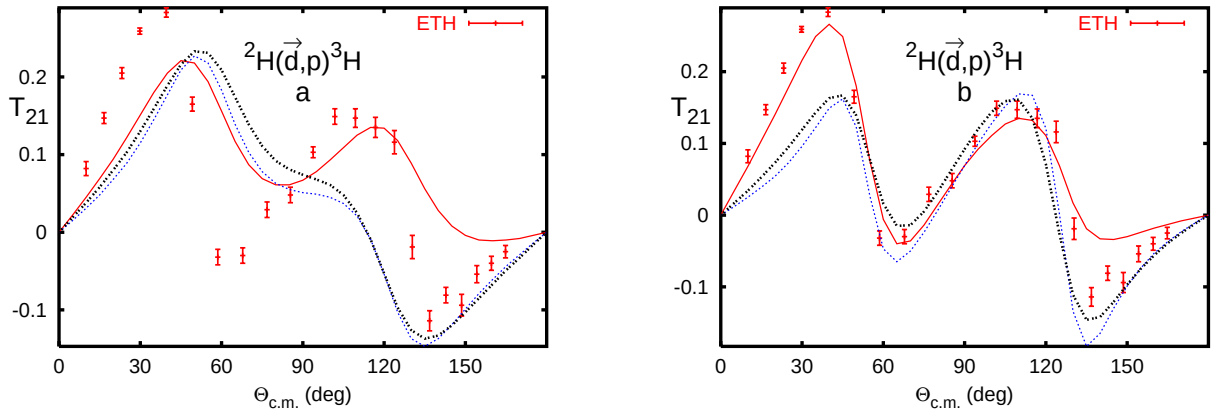

FIG. 23: (Color online) Same as fig. 21, but for the analyzing power T_{21} of the reaction ^{2}H$(d,p)^3$H

In fig. 23 we display the tensor analyzing power T_{21}. Without F-waves, only the R-matrix results are similar to the data. Below 90 degrees the RRGM results are close to the

R-matrix ones, being almost antisymmetric. The RRGM calculations show almost no effect of the TNF. The R-matrix analysis including F-waves reproduces the data well with the exception of around 135°, where it becomes not negative enough. The RRGM calculation reaches these data, but misses the steep rise from zero to the first maximum. The overall agreement is satisfactory.

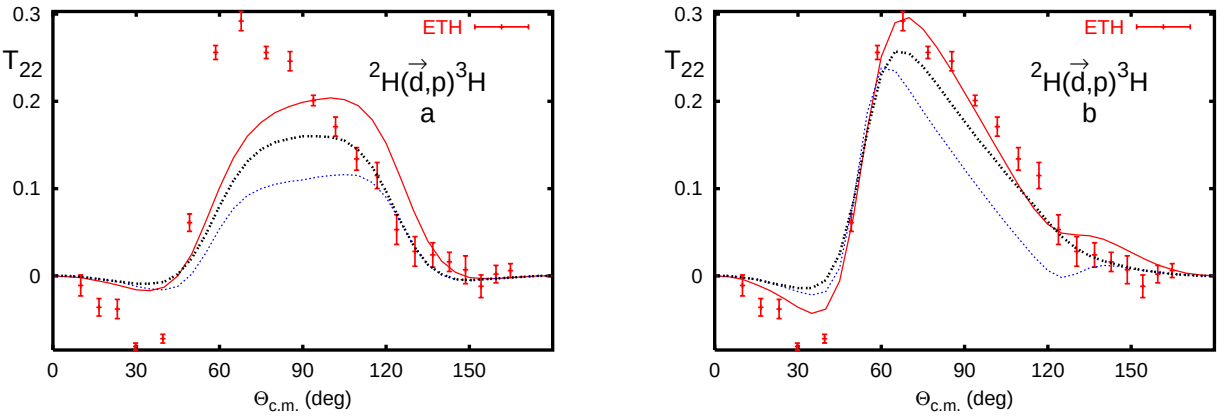

FIG. 24: (Color online) Same as fig. 21, but for the analyzing power T_{22} of the reaction ^{2}H$(d,p)^3$H

Without F-waves, the tensor analyzing power T_{22} shows again no qualitative agreement with the data, as shown in fig. 24. The R-matrix analysis and RRGM are all similar in shape; this holds also true when including F-waves. Again the R-matrix does a nice job, only underestimating the negative polarizations around 30 degrees. In this angular range the RRGM results are even less negative. Both calculations miss the height of the maximum, the NN force also the angle, and hence, also the falloff to zero, whereas including TNF yields reasonable agreement.

Let us now compare the results of the R-matrix analysis and the RRGM calculations in detail. All numerical work yields the $^3P_1$ and $^1D_2$ transition matrix elements as the largest ones, with the AV18 calculation creating the largest values; adding TNF, the typical loss is 10 percent, and the R-matrix ones are another 10 percent smaller. These ratios already take care of the forward-backward cross section behavior, as shown in fig. 20. The next larger matrix elements are much smaller, typically less than half the largest one. In the R-matrix analysis come the $^5S_2 \rightarrow {}^3D_2$ and then the $^1S_0$ transitions, whereas the RRGM yields the $^1S_0$ matrix element as the next larger. Adding the $^1S_0$ matrix elements keeps the cross sections as expected and still yields zero vector analyzing power since there is no second channel

with which to interfere. Adding the ${}^5S_2 \rightarrow {}^3D_2$ transition sets the scale for the maximum of the vector analyzing power. The R-matrix analysis gives the highest value, then the full RRGM calculation, and then NN forces only, as seen in fig. 21. Also this transition allows the tensor analyzing power T_{20} to approach its ultimate value around zero degrees, with the R-matrix giving the most negative value, which becomes somewhat more negative with increasing angle, before it reduces to the first maximum. The calculation including TNF yields a less negative value at 0°, becomes much more negative with increasing angle, until it also reduces to smaller values. The two RRGM calculations are quite similar to each other, with the AV18 calculation yielding always less negative values. Adding the next largest matrix element, which is the ${}^5D_1 \rightarrow {}^3D_1$ one for the R-matrix, leads to the saw-tooth structure for T_{21} (see fig. 23a), and the slightly negative values of T_{22} at small angles, followed by an increase, similar to fig. 24a. In the RRGM, this matrix element is only a quarter of the R-matrix size; therefore it plays no essential role. At this stage, however, the ${}^3P_2$ has to be taken into account. This matrix element leads to negative iT_{11} values similar to Fig. 21a, a behavior that is not changed by additional matrix elements. The resulting tensor analyzing powers T_{21} and T_{22} are still far from any qualitative structure of the data. Also adding the ${}^5S_2 \rightarrow {}^1D_2$ transition does not change the situation. Only when adding the ${}^3F_4$ and ${}^3F_3$ matrix elements, the RRGM reproduces qualitatively the data. The rest of the agreement of the final figs. 21, 22, 23, and 24 is due to the interplay of many more small matrix elements. One additional feature of the small matrix elements deserves mentioning: The ${}^5D_3 \rightarrow {}^3D_3$ matrix element in the RRGM calculation has the same magnitude, but opposite phase of the corresponding matrix elements coupled to total J of one or two. This sign change is in accordance with a dominating effective tensor force for this transition; however, the agreement with the polarization data becomes worse. In the R-matrix analysis this matrix element is essentially zero, and thus has no effect.

For the charge conjugate reaction ${}^2\mathrm{H}(d,n){}^3\mathrm{He}$, data exist from the Kentucky group [52] and the OSU group [53] at the same energy. Since charge symmetry is rather good, all data and calculations for the reaction ${}^2\mathrm{H}(d,n){}^3\mathrm{He}$ should be similar to those of ${}^2\mathrm{H}(d,p){}^3\mathrm{H}$, except for the small change in the energy of the exit channel. Therefore, we present only the results for the calculations including all channels. The OSU group measured the cartesian components of the analyzing powers; hence, for A_{xx} there is no direct counterpart in the proton channel, and we present also the results without F-waves taken into account. In

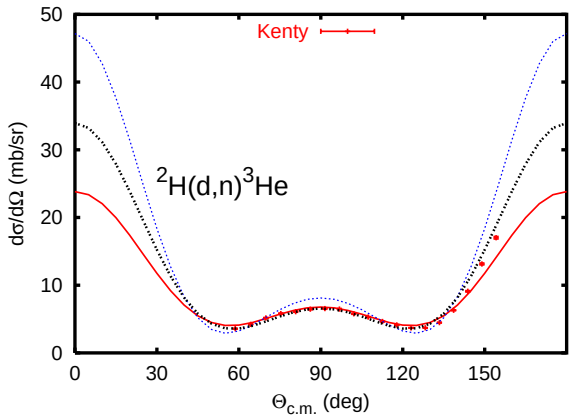

FIG. 25: (Color online) Differential cross section for the reaction $^2\mathrm{H}(d,n)^3\mathrm{He}$ calculated at 2.0 MeV E_{cm} with all matrix elements taken into account. For AV18 alone the energy is chosen that in the exit channel it agrees with the experimental one. The data from the Kentucky group [52] are at 2.0 MeV.

fig. 25 we compare the differential cross section data to the various calculations. As in the proton channel, the R-matrix analysis underestimates the backward data, the calculation using AV18 alone overestimates them, and including TNF brings the results in agreement with the data. Unfortunately the angular range of the data is rather limited.

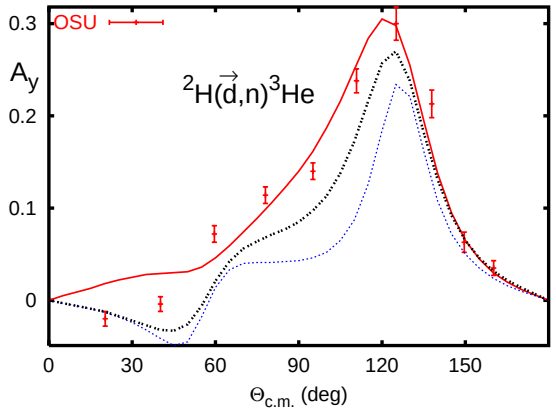

FIG. 26: (Color online) Same as fig. 25, but for the vector analyzing power A_y. The data are from the Ohio State group [53] at 2.0 MeV, as are all the following polarization data.

In fig. 26 we display the vector analyzing power A_y. The results of all calculations are quite similar to the proton calculations shown in Fig. 21b. The data of the OSU group [53] are slightly negative at forward angles, which the R-matrix analysis does not follow.

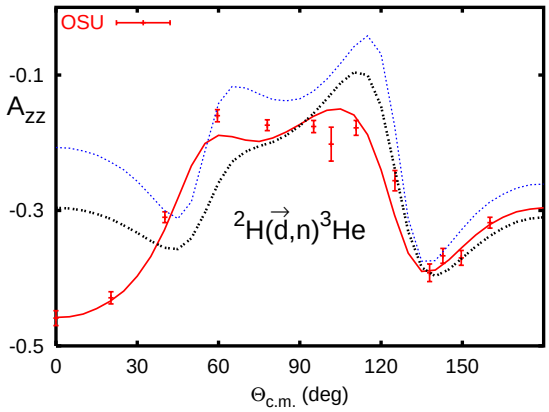

FIG. 27: (Color online) Same as fig. 26, but for the tensor analyzing power A_{zz}.

The R-matrix analysis reproduces the tensor analyzing power A_{zz} in fig. 27 very well, also at the extreme forward and backward angles. As in the proton channel, the RRGM calculations do not reach the minimum at zero degrees. Also the structure before the second maximum is not well reproduced. Some of the disagreement is due to the $^5D_3 \rightarrow {}^3D_3$ matrix element, as discussed above.

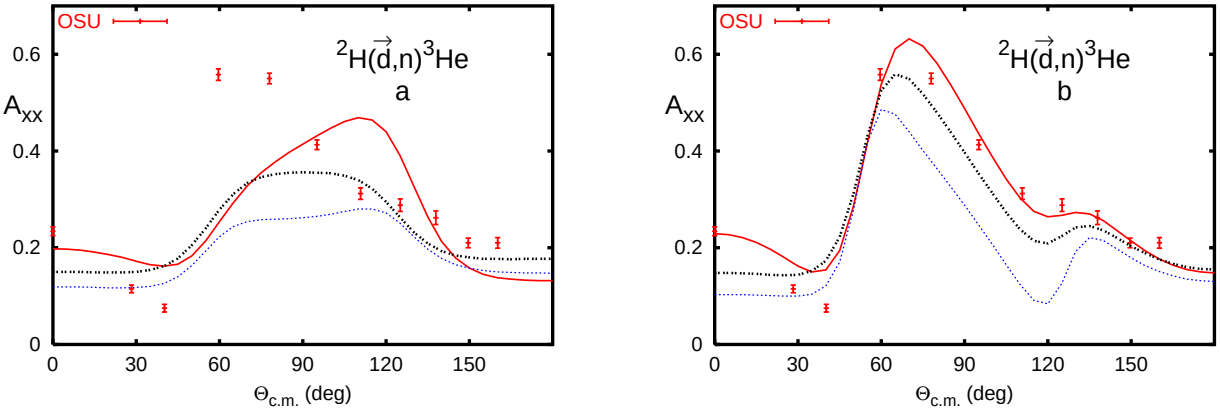

FIG. 28: (Color online) Same as fig. 26, but for the tensor analyzing power A_{xx}, F-waves are taken into account in (b), but not in (a).

Since the tensor analyzing power A_{xx} has no direct counterpart in the proton channel, we present in fig. 28 the results with and without F-waves. Without F-waves, the structure of the calculation does not reproduce the data, and only the R-matrix analysis gives qualitative agreement up to 60°. Including F-waves the R-matrix reproduces the data well, except close to thirty degrees. The RRGM calculations agree qualitatively with the data, with major

deficiencies below 30° and around 120°. The full calculation agrees better overall.

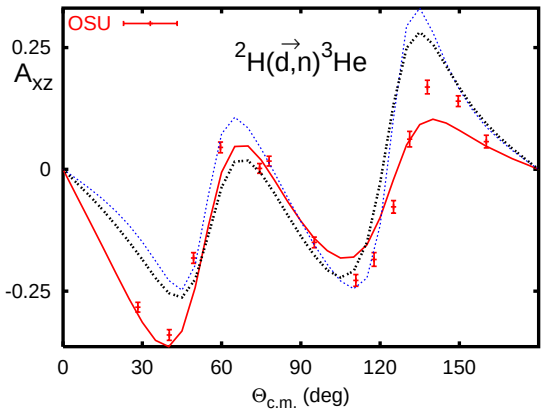

FIG. 29: (Color online) Same as fig. 26, but for the tensor analyzing power A_{xz}.

As for T_{21} of the proton channel, the saw-tooth structure of the tensor analyzing power A_{xz} is well reproduced by all the calculations. The R-matrix has some difficulties around 150°, and the RRGM results differ there and also around 45°. Note the sign difference between figures 29 and 23 due to the definition of A_{xz} and T_{21}.

Considering all results for the ^{2}H$(d,n)^3$He reaction, we find very close similarity with the charge conjugate proton channel. Some observables are better reproduced by the R-matrix analysis in the proton channel, others in the neutron channel. The parameter-free RRGM calculations do not reach a similar agreement for the analyzing powers. The transition matrix elements follow the same pattern as for the proton channel, although the small matrix elements usually have a somewhat larger effect.

One of the significant differences noted earlier between the R-matrix fit and the measurements was for the d - d reaction differential cross sections at forward and backward angles, even with the F-wave transitions included. In comparing with the RRGM calculations, which predict those cross sections much better, it appears that this difference comes primarily from the interference of the $^1S_0$ and $^1D_2$ transition matrix elements. The $^1S_0$ transition obtained from the R-matrix fitting has an interference effect between levels at low energies that does not show up in the RRGM calculations. Because of this interference effect, the phase of the transition element changes sign and gives the opposite interference behavior with the $^1D_2$ matrix element at most energies, compared with the RRGM calculations. This results in an important component of the "P_2" behavior of the differential cross section

having the opposite sign with respect to the calculations, giving cross sections that are too high at 90 degrees, and too low at forward and backward angles.

Earlier in the analysis, it was thought that the deficiency was due to the lack of higher partial waves. However, the comparison to the RRGM calculations reveals that the problem is likely this anomalous interference pattern in the 0^+ levels of the fit. We speculate that this behavior arose in order to give a rapid rise in the S-wave reaction cross sections at low energies, and is symptomatic of the d - d channel radius (7 fm) having too small a value.

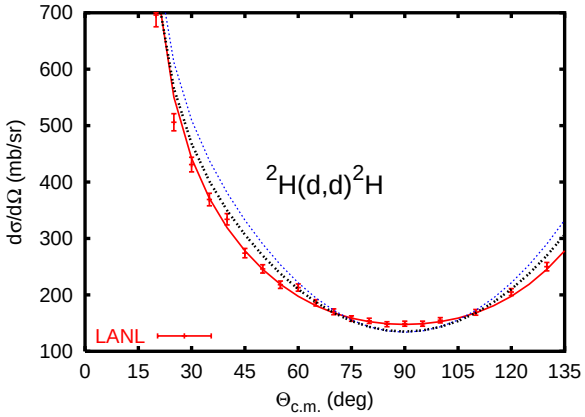

FIG. 30: (Color online) Differential cross section for elastic deuteron-deuteron scattering calculated at 3.0 MeV E_{cm} including F-waves. The data are from [54] at 3.0 MeV.

Let us now discuss the last two-body process, the elastic deuteron-deuteron scattering. Due to the identical bosons in entrance and exit channel, the vector analyzing power iT_{11} and the tensor analyzing power T_{21} are antisymmetric about 90°; all other observables are symmetric. Most of the existing data are unfortunately converted into the forward hemisphere, so that obvious violations of the symmetry are no longer visible, and artificial scatter might lead to the false interpretation of higher partial waves. Due to the small values of the polarization observables, the fact that we calculate them to only 3 significant places sometimes yields rough lines in the figures and does not allow the finest details of the calculations to be seen. Omitting F-waves in the full RRGM calculation yields at most unit changes in the last significant digit, which are too small to give any noticable change in the figures. Therefore we do not generally compare calculations with and without F-waves, but return to this point at the end of the section.

The R-matrix analysis reproduces the rather old differential cross section data [54] well,

considering the large error bars in fig. 30. The RRGM calculations do not reach the minimum at 90° and overshoot the data below 60°, with the full calculation being closer to the data.

In fig. 31 the rather small vector analyzing-power data are compared to the calculations. All calculations reproduce the small values with its relatively large errors. The R-matrix analysis shows structure that is not supported by the data. The effects of adding TNF are negligible. Note the much smaller scale compared to [10] here and in the following analyzing powers.

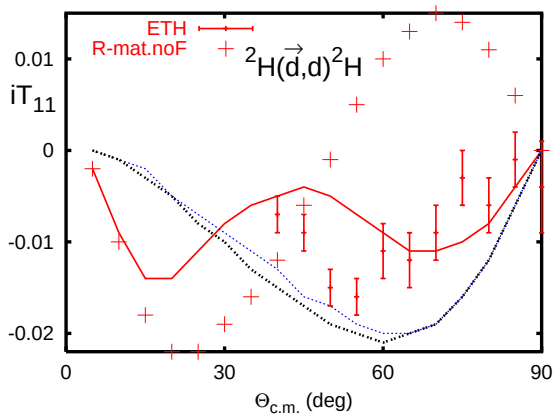

FIG. 31: (Color online) Vector analyzing power iT_{11} for elastic deuteron-deuteron scattering calculated at 3.0 MeV E_{cm}. The data are from the Zürich group [55] at 3.0 MeV, transfered into the forward hemisphere. The pluses are the R-matrix results omitting all F-wave contributions.

The tensor analyzing power T_{20} is one of the few variables with data also in the backward hemisphere. Fig. 32 shows the data of the Zürich group [55], with their scatter and large errors, and also the data of the TUNL group [56] with much smaller errors, covering the angular range up to 120°. The R-matrix analysis reproduces the data nicely, not quite reaching the maximum at ninety degrees. The RRGM calculation with AV18 alone misses the minimum around 45° by about a factor of two, but comes close to the maximal values. Adding TNF yields relatively large effects, coming close to the R-matrix results and data.

The T_{21} data of the Zürich group [55] show again considerable scatter in both the values and uncertainties as seen in fig. 33. All calculations reproduce these small polarizations reasonably well. The effects of TNF are again small.

For the tensor analyzing power T_{22} again exist data from the Zürich [55] and TUNL [56] groups. The Zürich data show a deep minimum at 90° with large relative errors, the TUNL

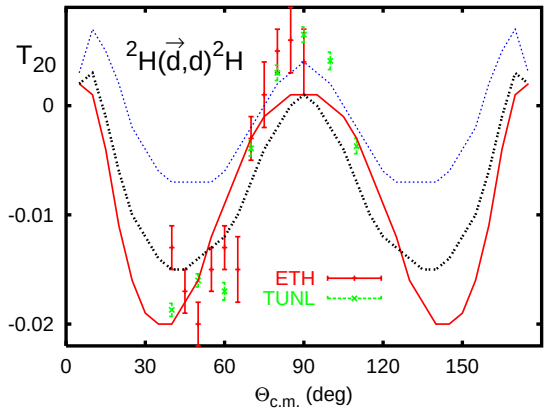

FIG. 32: (Color online) Same as fig. 31, but for the tensor analyzing power T_{20}. The data from the Zürich group [55] are transfered into the forward hemisphere, whereas the data of the TUNL group [56] are shown as taken.

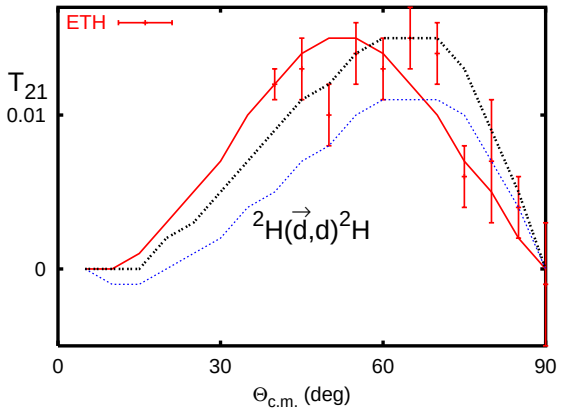

FIG. 33: (Color online) Same as fig. 31, but for the tensor analyzing power T_{21}.

data are about a factor of two smaller in the minimum with the errors about the same factor smaller, as seen in fig. 34. The R-matrix analysis yields small positive and negative values with no indication of the minimum. The two RRGM calculations are on top of each other and reproduce the TUNL data nicely.

Let us now discuss the differences in the various calculations. As mentioned before, the effects of F-waves in the RRGM calculations are negligible, so we did not compare those cases. As demonstrated in figs. 31, 32, 33, and 34, the effects of the TNF are small-to-negligible. For most observables, the full calculations in the R-matrix or RRGM framework yield similar results, especially if we take the smallness of the polarization values

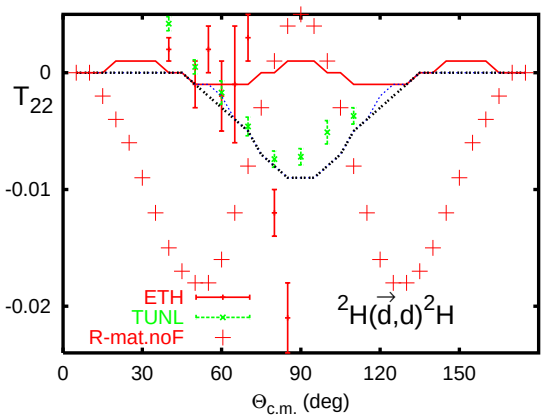

FIG. 34: (Color online) Same as fig. 32, but for the tensor analyzing power T_{22}. In addition the results of the R-matrix analysis omitting F-wave contributions are shown as '+'.

into account. If we look at individual partial waves, however, this apparent agreement breaks down. Omitting the F-waves in the R-matrix analysis yields no effect in the differential cross section, small changes for the T_{21} angular distribution, a shallower minimum and maximum for T_{20}, and large modifications for the rest. The angular distribution of the vector analyzing powers iT_{11} becomes $\sin(4\Theta)$ with a minimal value of -0.022, as shown by the pluses in fig. 31, whose remnants are still visible in the final result. For T_{22}, the effects of omitting the F-waves are displayed in fig. 34. This suggests that the F-waves are neccessary for some of the polarizations to compensate for artifacts introduced by the lower partial waves. As mentioned in the previous section for the D-wave and P-wave phase shifts and displayed in figs. 8, 12, and 13 for D-, P-, and F-waves, the R-matrix analysis finds considerable J-splitting, whereas the RRGM calculations do not support these findings. It is unclear at this point which data cause this large J-splitting. The origin of this problem are the very few data in the backward hemisphere. Transforming the original backward hemisphere ETH-data into the forward hemisphere might have introduced this artificial behaviour.

With the knowledge of the scattering and bound-state wave functions, various radiative capture reactions can be calculated, at least in the long-wave-length limit, for the complex RRGM wave functions used here. For the reaction ^{2}H(d,γ)^{4}He, new data at very low energies exist from the TUNL group, which are well reproduced, together with older data of this reaction by a calculation similar to the one described above [57]. Further work on the proton and neutron capture reactions is under way [58]. Unfortunately for these reactions,

the data situation is very controversial; see the recent calculation compared to data [59].

Data needs and conclusion

The R-matrix analysis uses many more data than discussed in the previous section to determine the R-matrix parameters. Using these, it is possible to interpolate or even extrapolate to energies where no data for the elastic scattering or specific reaction are available, or to predict polarization observables that have not been measured so far. We have chosen the energies presented here by the requirement to have a maximum number of data sets at this energy.

Compared to the previous calculations using the Bonn potential [10], the agreement between the parameter free RRGM calculation using the Argonne v18 two-nucleon potential and the R-matrix analysis and data is much better. The partial wave analysis allows to point to specific features that need further studies, and additional or improved data. Due to the complexity of the A=4 system, we cannot specify which part of the two- or three-nucleon potential causes the differences seen in the previous sections. Therefore, we can only point out which effective two-body interaction might be responsible.

Let us assume for the moment that the R-matrix is equivalent to the data; then we can conclude from figs. 4, 5, and 7, that all the S-waves are very well reproduced and thus there is almost no room left for modifications of the central force. The 0^+ triton-proton phase shift below the neutron threshold might be the exception, which was used in [26] together with the very low-energy data in ^{3}He-neutron scattering and the ^{3}He(n,p)^{3}H reaction, to advocate a slight reduction of the long-range and slight increase of the short-range part of the central force. The good agreement for the singlet P- and D-waves (see figs. 10 and 6, 7 respectively), supports this further, whereas the $^1F_3$ triton-proton and ^{3}He-neutron phase shifts disagree widely between R-matrix analysis and RRGM calculation.

The deuteron-deuteron triplet P-waves indicate a rather strong spin-orbit force in the R-matrix analysis, which is not quite met in the RRGM calculation, as seen in fig. 12. The [3 + 1] triplet P-waves show a smaller J-splitting in the R-matrix analysis that the RRGM calculation follows nicely, without quite reaching the values for the $^3P_1$ and $^3P_2$ phase shifts for the higher energies. This mismatch also leads to differences in the energy dependence, especially for the 0^- channel.

For the higher partial waves, which are small in the R-matrix analysis and the RRGM calculation, relatively large differences occur. Whereas the RRGM calculation reveals the dominance of the central force component by only a very weak J-splitting in the elastic phase shifts, the R-matrix analysis yields an appreciable splitting, the origin of which is still unclear.

Let us now compare directly to data. As mentioned in the previous section, the [3 + 1] elastic scatterings and reactions are very sensitive to P-wave matrix elements. The difference between the polarization of the heavy fragment and the light one depends only on triplet-singlet transition matrix elements, thus essentially singling out the ${}^3P_1 \longrightarrow {}^1P_1$ matrix element. Since we realize that experiments with triton beams or targets are now problematic, we consider the reaction ^{3}He(n,p)^{3}H the perfect choice. Around 8 to 10 MeV neutron energy it would add to the already existing elastic scattering data, and thus via unitarity, lead to a much more restrictive analysis. Taking only the strongest transitions into account, R-matrix and RRGM calculations yield widely different predictions for cross sections and analyzing powers. Also, the TNF play a large role, due to the very large 0^- matrix element. The cross section at forward angles differs by thirty percent. Therefore, the energy region around the broad second 0^- resonance [13] is of great interest.

For d - d elastic scattering, a few recent polarization data are available [56] that contradict to a large extent the older ones. In order to reduce the weight of the existing iT_{11} and T_{21} at higher energies, new data would be highly welcome, preferably in the backward hemisphere. Especially also cross section data with smaller errors should improve the analysis and allow for a better comparison between the various three-nucleon potentials.

The deuteron–deuteron fusion reactions are a very special case. Since there the F-waves play a large role, they are essential in determining these partial waves. Unfortunately the cross section data do not cover the very forward and backward regions; hence, the R-matrix analysis is not forced to reproduce these angle ranges. A few cross section measurements for both outgoing channels would improve the situation tremendously. Also the dependence on the TNF is very strong at the extreme angles, as seen in figs. 20 and 25.

The polarization data of the proton channel are taken at almost twice as many angles as are the neutron channel data. Since the relative errors are comparable, the weight of the proton data is much higher in the analysis. The forward region (for T_{21}/A_{xz}, the backward hemisphere) poses the main problem to the R-matrix analysis. Especially for iT_{11} and T_{20},the

differences between the charge conjugate channels are large, which is not to be expected due to charge symmetry. The differences due to the different thresholds are essentially given by the variations of the RRGM calculations. Three-nucleon forces yield large enough effects to make these polarizations a valuable tool to determine TNF.

Before closing, we want to add a few remarks about the A_y problem encountered in deuteron-nucleon and proton-^{3}He elastic scattering and not seen here in the ^{4}He system. Since the mismatch between the maximal analyzing power of the data and the calculations, for example using AV18 and UIX, is much larger for the p - ^{3}He scattering than for deuteron-nucleon scattering, one might be tempted to conclude that the origin of this deficiency is a missing $T = 1$ force component. But then it should also show up in the [3 + 1] channels considered here, which it does not. This contradiction can be resolved by noting, that in the previous cases the triplet P-waves matrix elements showed small J-spitting and had (essentially) modulus one. Here, however, we find an appreciable J-splitting and due to channel coupling, moduli much smaller than one, thus leading to a much more complex behavior of the analyzing powers.

We have shown in this paper how well an R-matrix analysis of the data can represent them by a relatively small number of R-matrix parameters. In addition to that, a parameter-free RRGM calculation allowed to show the agreement with results from the Argonne v18 two-nucleon potential only and the effects of the additional Urbana IX TNF. These effects are quite large for some partial waves or specific data. Therefore, we consider the ^{4}He system a good place to study the effects of TNF and to use the comparison with data in order to determine the structure and radial dependence better. To learn more about the TNF, other forces, like the Tucson-Melbourne force [60] in its modified form [61], or one from effective field theories [62] have to be applied also. Unfortunately, the RRGM calculations are very time consuming, especially when the TNF is included. Since every spin-isospin operator has to be programmed individually (and the radial dependence expanded in terms of Gaussians), the recent Illinois force [63] is currently on the verge of feasibility [64]. The most accessible seems to be the Tucson-Melbourne force [61], which contains no new operator compared to the Urbana IX force used here. We plan a new calculation using this force. The potentials derived from effective field theories can only be used when a reliable configuration-space version is available.

Despite the above plea for additional and improved data, we consider the whole set of

data in the ^{4}He system well suited to study the three-nucleon forces. On the one hand there are clear-cut structures that vary only slowly with energy, but in the reactions we found energy regions with a rapid change in the observables, which could be used for a fine-tuning of the TNI. To be not mislead by incorrect data, a procedure similar to the approach of the Nijmegen-Group for the nucleon-nucleon data has to be carried out. With the knowledge of the differences between the R-matrix analysis and the microscopic calculation, we have started a new R-matrix analysis, where we use initially only a few data sets, omitting all the suspicious ones with high χ^2 values, and constraining the fit to give smaller J-splittings. Then we plan to add more and more data sets, in order to learn which of them cause the J-splitting found so far. The results of this tedious procedure will be published elsewhere.

Note added in proof: After completion of the manuscript, we became aware of the work of A. C. Fonseca et al. [65, 66], in which they use various NN-potentials, and come to similar results as we do for the AV18. However, the many-nucleon force [66] they include via Δ-excitation behaves differently from the UIX potential that we have used.

Acknowledgments

This work is supported by the DFG under HO 780/9 and used resources at several computer centers (RRZE Erlangen and HLRB München). We want to thank G. Wellein and G. Hager at the RRZE for their help. The U. S. Department of Energy supported the work of G. M. H. on this study.

---

[1] V. G. J. Stoks, R. A. M. Klomp, M. C. M. Rentmeester, and J. J. de Swart, Phys. Rev. **C48**, 792 (1993).

[2] A. Kievsky, S. Rosati, W. Tornow, and M. Viviani, Nucl. Phys. **A607**, 402 (1996).

[3] H. Witala, D. Hüber, and W. Glöckle, Phys. Rev. **C49**, R14 (1994).

[4] A. Kievsky and W. Tornow, TUNL Progress Report - XXXVIII, TUNL, Durham, USA (1999).

[5] H. Witala, W. Glöckle, J. Golak, A. Nogga, H. Kamada, R. Skibinski, and J. Kuroś-Żołnierczuk, Phys. Rev. **C63**, 024007 (2001).

[6] J. K. Żołnierczuk et al., Phys. Rev. **C66**, 024003 (2002).

[7] J. K. Żołnierczuk et al., Phys. Rev. **C66**, 024004 (2002).

[8] I. Fachruddin, C. Elster, and W. Gloeckle, Phys. Rev. **C68**, 054003 (2003).

[9] M. Viviani, S. Rosati, and A. Kievsky, Phys. Rev. Lett. **81**, 1580 (1998).

[10] H. M. Hofmann and G. M. Hale, Nucl. Phys. **A613**, 69 (1997).

[11] F. Ciesielski, J. Carbonell, and C. Gignoux, Phys. Lett. **B447**, 199 (1999).

[12] R. Lazauskas and J. Carbonell, Few-Body Systems **34**, 105 (2004).

[13] D. R. Tilley, H. R. Weller, and G. M. Hale, Nucl. Phys. **A541**, 1 (1992).

[14] G. M. Hale (2003), unpublished.

[15] R. Machleidt, K. Holinde, and C. Elster, Phys. Rep. **149**, 1 (1987).

[16] H. Kellermann, H. M. Hofmann, and C. Elster, Few-Body-Systems **7**, 31 (1989).

[17] K. Wildermuth and Y. C. Tang, *A Unified Theory of the Nucleus* (Vieweg, 1977).

[18] Y. C. Tang, in *Topics in Nuclear Physics* (Springer, 1981), vol. 145 of *Lecture Notes in Physics*.

[19] H. M. Hofmann, in *Proceedings of Models and Methods in Few-Body Physics, Lisboa, Portugal 1986*, edited by L. S. Ferreira, A. C. Fonseca, and L. Streit (1987), vol. 273 of *Springer Lecture Notes in Physics*, p. 243.

[20] W. Kohn, Phys. Rev. **74**, 1763 (1948).

[21] R. B. Wiringa, V. G. J. Stokes, and R. Schiavilla, Phys. Rev. **C51**, 38 (1995).

[22] B. S. Pudliner, V. R. Pandharipande, J. Carlson, S. C. Pieper, and R. B. Wiringa, Phys. Rev. **C56**, 1720 (1997).

[23] L. Canton and W. Schadow, Phys. Rev. **C62**, 044005 (2000).

[24] B. Pfitzinger, H. M. Hofmann, and G. M. Hale, Phys. Rev. **C64**, 044003 (2001).

[25] H. M. Hofmann and G. M. Hale, nucl-th/0211008 (2002).

[26] H. M. Hofmann and G. M.Hale, Phys. Rev. **C68**, 021002(R) (2003).

[27] C. Winkler and H. M. Hofmann, Phys. Rev. **C55**, 684 (1997).

[28] A. Nogga, H. Kamada, and W. Glöckle, Phys. Rev. Lett **85**, 944 (2000).

[29] A. C. Fonseca, Phys. Rev. Lett. **83**, 4021 (1999).

[30] J. Als-Nielsen and O. Dietrich, Phys. Rev. **133B**, 925 (1964).

[31] L. A. Physics and C. Groups, Nucl. Phys. **12**, 291 (1959).

[32] B. Haesner, W. Heeringa, H. O. Klages, H. Dobiasch, G. Schmalz, J. Wilczinski, B. Zeitnitz, and F. Kaeppler, Phys. Rev. C **28**, 995 (1983).

[33] C. D. Keith, D. Rich, and W. M. Snow (2003), private communication.

[34] V. P. Alfimenkov, S. B. Borzakov, V. V. Tkhuan, A. M. Govorov, L. Lason, L. B. Pikel'ner,

and E. A. Sharapov, Yad. Fiz. **33**, 891 (1981), english trans.: Sov. J. Nucl. Phys. **33**, 467 (1981).

[35] J. H. Gibbons and R. L. Macklin, Phys. Rev. **114**, 571 (1959).

[36] C. R. Brune, K. I. Hahn, R. W. Kavanagh, and P. R. Wrean, Phys. Rev. C **60**, 015801 (1999).

[37] G. M. Hale, R. E. Brown, and N. Jarmie, Phys. Ref. Lett. **59**, 763 (1987).

[38] P. E. Koehler, C. D. Bowman, F. J. Steinkruger, D. C. Moody, G. M. Hale, J. W. Starner, S. A. Wender, R. C. Haight, P. W. Lisowski, and W. L. Talbert, Phys. Rev. **C37**, 917 (1988).

[39] A. C. Fonseca, G. Hale, and J. Haidenbauer, Few-Body Systems **31**, 139 (2002).

[40] R. Detomo and T. Donoghue (1978), unpublished, Ohio State University.

[41] R. Kankowsky, J. C. Fritz, K. Kilian, A. Neufert, and D. Fick, Nucl. Phys. **A263**, 29 (1976).

[42] R. F. Haglund, Jr., R. E. Brown, N. Jarmie, G. G. Ohlsen, P. A. Schmelzbach, and D. Fick, Phys. Lett. **B79**, 35 (1978).

[43] J. E. Perry, Jr. (1959), unpublished, reported by J. D. Seagrave, in: Proc. Conf. on Nuclear Forces and the Few Nucleon Problem, London.

[44] P. R. Huffman, D. L. Jacobson, K. Schoen, M. Arif, T. C. Black, W. M. Snow, and S. A. Werner, Phys. Rev. **C70**, 014004 (2004).

[45] O. Zimmer et al., EPJdirect **A1**, 1 (2002).

[46] F. Kohlrausch, ed., *Praktische Physik, Bd.3, Neutronenstreulängen und Wirkungsquerschnitte* (Teubner, 1996), p. 544.

[47] M. Drosg, D. K. McDaniels, J. C. Hopkins, J. D. Seagrave, R. H. Sherman, and E. C. Kerr, Phys. Rev. **C9**, 179 (1974).

[48] B. Haesner (1995), dissertation, KFZ Karlsruhe (1982); priv. com. by H. Klages.

[49] L. Drigo, G. Tornielli, and G. Zannoni, Ann . Phys. **39**, 408 (1982).

[50] P. W. Lisowski, C. T. Rhea, and R. L. Walter, **A259**, 61 (1976).

[51] W. Grüebler, V. König, P. A. Schmelzbach, R. Risler, R. E. White, and P. Marmier, Nucl. Phys. **A 193**, 129 (1972).

[52] R. L. Schulte, M. Cosack, A. W. Obst, and J. L. Weil, Nucl. Phys. **A 192**, 609 (1972).

[53] L. J. Dries, H. W. Clark, R. Detomo, Jr., and T. R. Donoghue, Phys. Lett. **B 80**, 176 (1979).

[54] J. E. Brolley, Jr., T. M. Putnam, L. Rosen, and L. Stewart, Phys. Rev. **117**, 1307 (1960).

[55] W. Grüebler, V. König, R. Risler, P. A. Schmelzbach, R. E. White, and P. Marmier, Nucl. Phys. **A 193**, 149 (1972).

[56] B. J. Crowe, III, C. R. Brune, W. H. Geist, H. J. Karwowski, E. J. Ludwig, K. D. Veal, A. C. Fonseca, G. M. Hale, and K. A. Fletcher, Phys. Rev. **C61**, 034006 (2000).

[57] K. Sabourov, M. W. Ahmed, R. S. Canon, B. Crowley, K. Joshi, J. H. Kelley, S. O. Nelson, B. A. Perdue, E. C. Schreiber, A. Sabourov, et al., Phys. Rev. **C 70**, 064601 (2004).

[58] M. Trini, Ph.D. thesis, Erlangen (2006).

[59] S. Quaglioni, W. Leidemann, G. Orlandini, N. Barnea, and V. D. Efros, Phys. Rev. **C69**, 044002 (2004).

[60] S. A. Coon, M. D. Scadron, P. C. McNamee, B. R. Barrett, D. W. E. Blatt, and B. H. J. McKellar, Nucl.Phys. **A317**, 242 (1979).

[61] S. A. Coon and H. K. Han, Few-Body Systems **30**, 131 (2001).

[62] U. van Kolck, Phys. Rev. **C49**, 2932 (1994).

[63] S. C. Pieper, V. R. Pandharipande, R. B. Wiringa, and J. Carlson, **C64**, 014001 (2001).

[64] J. Kirscher, Master's thesis, Erlangen (2006).

[65] A. Deltuva and A. C. Fonseca, Phys. Rev. **C76**, 021001 (2007).

[66] A. C. F. A. Deltuva and P. U. Sauer, nucl-th/0801.2743 (2008).